JOURNAL OF GEOPHYSICAL RESEARCH, VOL. 114, C06024, doi:10.1029/2008JC004742, 2009

Computation and approximation of the length scales of harmonic modes with application to the mapping of surface currents in the Gulf of Eilat

F. Lekien[1] and H. Gildor[2]

Received 17 January 2008; revised 9 January 2009; accepted 28 January 2009; published 26 June 2009.

[1] Open-boundary modal analysis (OMA) is a generalized Fourier transform that interpolates, extrapolates, and filters scattered current measurements and produces smooth current maps in coastal areas. Boundary conditions are enforced by adjusting the OMA modes to the coastline. Filtering is achieved by discarding OMA modes whose length scales are below a selected threshold. In this paper, we determine the length scale of the OMA modes, and we derive approximated formulas. Operational use of the OMA modes and the length scale formulas are illustrated on surface currents measured by high-frequency radar in the Gulf of Eilat (Gulf of Aqaba).

Citation: Lekien, F., and H. Gildor (2009), Computation and approximation of the length scales of harmonic modes with application to the mapping of surface currents in the Gulf of Eilat, *J. Geophys. Res.*, *114*, C06024, doi:10.1029/2008JC004742.

1. Introduction

[2] Increasingly accurate remote sensing techniques are available for measuring surface currents in coastal areas [*Barrick et al.*, 1985; *Gurgel et al.*, 1999b]. High-frequency (HF) radar stations measuring surface currents, such as the SeaSonde [*Hodgins*, 1994] or WERA [*Gurgel et al.*, 1999a] flourish along shorelines worldwide. On the basis of Bragg resonance from ocean waves and the Doppler shift in the reflected signal, the HF radar station is able to determine the magnitude of the surface current along a radial joining the antenna and any target point [*Barrick et al.*, 1977]. For a given location, measured radial currents (henceforth "radials") from at least two different angles are needed to evaluate directly the surface velocity vector (henceforth "total").

[3] Figure 1 describes the setting in the Gulf of Eilat in the northern Red Sea. Two 42 MHz SeaSonde HF radar systems measure the currents at a spatial resolution of approximately 300 m and a temporal resolution of 30 min. There is one SeaSonde at the InterUniversity Institute in Eilat (IUI) and another station at the Port of Eilat (PORT). The distance between the two stations is approximately 5 km. In order to approximate the current vector at a certain point, we need to have radials measurements from both stations and the two should observe this patch of water from different angles. Ideally, we want an angle of about 90° between the two radials and, in any case, at least 15° [*Barrick*, 2002].

[4] In addition to geometric considerations, such as the distance from the radar stations and the angle between the radials, the accuracy of the measurement is also subject to sea conditions and radio frequency noise levels. As a result, the output of such a sensing system is a time varying cloud of radial measurements. Not only are the radial currents changing over time but also their number, locations and accuracy.

[5] For practical purposes such as tracking algae blooms [*Olascoaga et al.*, 2006] or maximizing the dispersion of pollutants [*Lekien et al.*, 2005], it is necessary to fill the gaps in the data and to control its quality. Several methods are available to interpolate and extrapolate the radar data: one may perform objective mapping [*Kim et al.*, 2007], use empirical orthogonal functions (EOF) or use Fourier transforms. An invaluable advantage of the latter is that the currents are written as a sequence of modes, each of which with a specific length scale. Filtering can therefore be performed by thresholding the wavelength of the modes.

[6] A disadvantage of the standard Fourier transform is its inadequacy in coastal areas. Indeed, currents developed in a Fourier basis will not necessarily be tangent to a coastline. While this may not be a significant problem in Eulerian studies, any method based on Lagrangian paths suffers dramatically from such a violation of the boundary conditions [*Coulliette et al.*, 2007]. Whether one integrates single particle paths, computes finite-time stretching, or extracts Lagrangian coherent structures, it is critical to start from surface currents that are tangent to the coastline and that will not allow particle trajectories to penetrate the coastline.

[7] The work of *Lynch* [1989] and *Eremeev et al.* [1992a, 1992b] generalizes the notion of Fourier modes to a coastal domain with an arbitrary coastline. Instead of projecting on products of sines and cosines, the modes are defined as the eigenfunctions of the Laplacian for the domain of interest [*Lipphardt et al.*, 2000]. *Lekien et al.* [2004] show that this

[1] École Polytechnique, Université Libre de Bruxelles, Brussels, Belgium.
[2] Department of Environmental Sciences and Energy Research, Weizmann Institute of Science, Rehovot, Israel.

0148-0227/09/2008JC004742$09.00

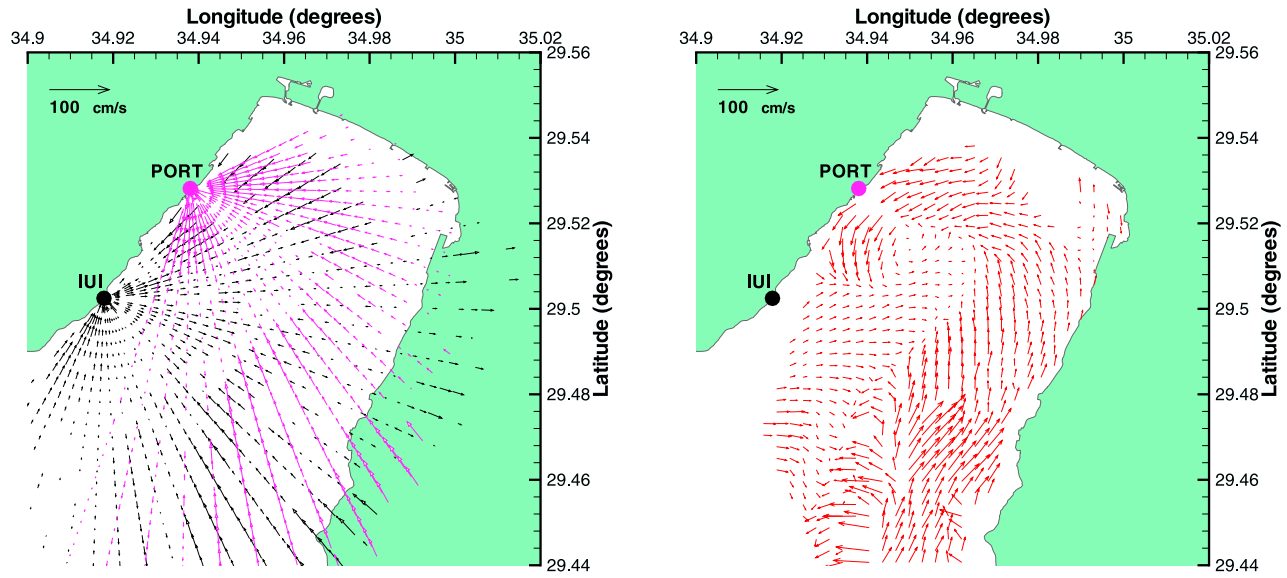

Figure 1. (left) Radial currents on 29 November 2005 at 1000 UT from the stations PORT (purple) and IUI (black). (right) Approximated total vectors are computed in regions where radial coverage in two distinct directions is available. In order to directly compute the total vector from the radials measurements, we need to combine nearby radials from at least two different angles. As a result, there are always more radial measurements than computed vector components.

generalized Fourier basis is complete: it can represent all possible surface currents and it guarantees that the currents are tangent to the coastline. *Lekien et al.* [2004] further add a new sequence of open-boundary modes to allow inflow and outflow through the segments of the boundary that are not part of the coastline.

[8] This procedure is referred to as open-boundary modal analysis (OMA). Each OMA mode is associated with a specific wavelength, or length scale. Being able to approximate this length scale quickly is essential when performing filtering or reconstruction of the currents. As shown by *Lekien and Coulliette* [2007], knowledge of accurate length scales for OMA modes also provides a premium method for computing quasi-turbulent energy spectra.

[9] The goal of this study is to derive robust formulas to compute the length scale of each OMA mode. Indeed, it is a necessary step to enable efficient filtering of the data and accurate nowcasting. Following *Tricoche et al.* [2001] and X. Tricoche (Topology simplification for turbulent flow visualization, paper presented at Grafiktag, Gesellschaft für Informatik, Saarbrücken, Germany, 2002), we investigate the OMA modes and derive their length scale on the basis of their features. For a given mode, we extract the width of the eddies contained in the mode. By eddy, we mean a closed contour of the stream function or the velocity potential. This "eddy" usually does not correspond to a real eddy in the current field but represents the smallest feature (length scale) of the observed mode. We then derive several approximations and compare them with existing formulas (namely, the expressions used by *Lipphardt et al.* [2000] and *Lekien et al.* [2004]).

[10] Using our approximated formulae for the mode length scales, we investigate reconstruction of surface currents for the Gulf of Eilat. Because the gulf is a nearly rectangular basin, with only one segment of open boundary, it provides an ideal test site for the use of OMA modes, and for studying the influence of the mode wavelength and the grid resolution on the mapped currents. The analogy between the Gulf of Eilat and a rectangle enables us to demonstrate the correspondence between the approximated length scale formulas developed in this manuscript and the length scales of the more familiar Fourier modes. The results indicate that even in a relatively simple domain, a significant amount of modes is needed to accurately reconstruct the surface flow (several hundreds of modes at least).

2. Modal Analysis

[11] Following *Kaplan and Lekien* [2007], we decompose the two-dimensional velocity field as

$$\mathbf{v}(\mathbf{x},t) = \nabla \times (\mathbf{k}\,\psi) + \nabla\phi,$$

where ψ is the stream function, ϕ is the velocity potential and $\mathbf{k}$ is a unit vector orthogonal to the ocean plane. In most geophysical flows, a free-slip boundary condition is applied at the boundary of the domain (i.e., $\mathbf{n}\cdot\mathbf{v} = 0$ where $\mathbf{n}$ is a unit vector normal to the boundary). We enforce the boundary condition by requiring $\mathbf{t}\cdot\nabla\psi = \mathbf{n}\cdot\nabla\phi = 0$. Notice that $\mathbf{t}\cdot\nabla\psi = 0$ implies that ψ is constant along the boundary. We can therefore assume, without loss of generality, that $\psi = 0$ along the boundary.

[12] For many flow problems on a rectangle, one can further represent the stream function as an infinite sequence of Fourier modes

$$\psi(x,y,t) = \sum_{i,j=1}^{\infty} a_{ij}(t)\ \underbrace{\sin\left(i\pi\frac{x}{L}\right)\sin\left(j\pi\frac{y}{W}\right)}_{\psi_{ij}},$$

where L and W are the length (longest dimension) and width (shortest dimension) of the rectangular box.

[13] Similarly, the velocity potential can be expanded as

$$\phi(x,y,t) = \sum_{\substack{i,j=0 \\ (i,j)\neq(0,0)}}^{\infty} b_{ij}(t) \underbrace{\cos\left(i\pi\frac{x}{L}\right)\cos\left(j\pi\frac{y}{W}\right)}_{\phi_{ij}} .$$

[14] A valuable property of the Fourier decomposition is the fact that each term satisfies, independently, the boundary condition. As a result, one can modify the coefficients $a_{ij}(t)$ and $b_{ij}(t)$ freely without any impact on the global boundary condition. Experimental and numerical errors on the coefficients $a_{ij}(t)$ and $b_{ij}(t)$ do not have any effect on the global boundary condition.

[15] Open-boundary modal analysis is a generalized Fourier transform for domains that are not rectangular. Given a compact domain Ω and its boundary $\partial\Omega$, the generalized stream function modes are defined by the functional eigenvalue problem with Dirichlet boundary conditions

$$\Delta\psi_n = -\lambda_n^2\,\psi_n \quad \text{inside } \Omega \quad \text{and} \quad \psi_n = 0 \text{ on } \partial\Omega .$$

The generalized potential modes are defined as the solutions of the Neumann eigenvalue problem

$$\Delta\phi_n = -\lambda_n^2\,\phi_n \quad \text{inside } \Omega \quad \text{and} \quad \mathbf{n}\cdot\nabla\phi_n = 0 \text{ on } \partial\Omega.$$

[16] In both cases, we ignore the trivial and constant eigenmodes corresponding to zero eigenvalues. If the domain Ω is a rectangle, the definitions above reduce to the Fourier modes. They are, however, applicable to any geometry and they provide free-slip modes also when the domain is not a rectangle. Standard results in functional analysis guarantee that any smooth (or piecewise smooth) stream function $\psi(\mathbf{x}, t)$ vanishing at the boundary $\partial\Omega$ can be written as

$$\psi(\mathbf{x},t) = \sum_{n=1}^{\infty} a_n(t)\,\psi_n(\mathbf{x}).$$

where ψ_n are the generalized Dirichlet modes. Similarly, any smooth velocity potential whose normal derivative vanishes at the boundary can be written as a linear combination of the generalized Neumann modes

$$\phi(\mathbf{x},t) = \sum_{n=1}^{\infty} b_n(t)\,\phi_n(\mathbf{x}).$$

[17] When the domain is not a rectangle, the modes can be computed using the finite element method [*Aubin*, 2000] and Arnoldi iterations [*Arnoldi*, 1951; *Lehoucq et al.*, 1998] to solve the resulting generalized eigenvalue problem. Selected Dirichlet and Neumann modes for the Gulf of Eilat are shown in Figure 2. Note that while the gulf is almost rectangular, the OMA modes are very different from Fourier modes. Indeed, the modes are known to change strongly in response to perturbations when their corresponding eigenvalues are close to the next eigenvalue [*Golub and Van Loan*, 1996]. Close to a rectangular shape (with its repeated eigenvalues), the modes then vary a lot under perturbation of the boundary.

[18] Note that the sensitivity of each individual OMA modes to perturbations of the boundary is not an issue as the ensemble of the modes continue to span the same velocity space [*Trefethen and Betcke*, 2006].

[19] Another observation to make about Figure 2 is the fact that the OMA modes do not contain closed contours with highly anisotropic length scales. In comparison, Fourier modes

$$\psi_{ij} = \sin\left(i\pi\frac{x}{L}\right)\,\sin\left(j\pi\frac{y}{W}\right),$$

where i is small and j is large, have long anisotropic contours. An advantage of OMA (and of working in a region with a complex boundary) is therefore the fact that each mode is associated with a very narrow band of length scales.

[20] The modal decomposition presented above is valid only for domains that are completely closed by a shoreline; there cannot be any flux of fluid through the boundary of the domain. In most practical applications and, in particular, for coastal studies, the domain freely exchanges particles and energy through segments of the boundary. For example, the southwestern edge of the domain depicted in Figure 2 is not a material coastline and the flow should let particles go freely across this "open boundary." As shown by *Lekien et al.* [2004], new modes can be introduced to span the degrees of freedom corresponding to the flow on the open boundary. If we consider the sequence of modes defined by

$$\Delta\phi_n^b = \frac{\oint_{\partial\Omega} g_n(s)\,\mathrm{d}s}{\mathrm{Area}(\Omega)} \text{ inside } \Omega \quad \text{and} \quad \mathbf{n}\cdot\nabla\phi_n^b = g_n(s) \text{ on } \partial\Omega,$$

where $\{g_n(s)\}$ is a basis for the functions defined on the open boundary. Any velocity field, that is tangent to the coastline and arbitrary along the open boundary, can then be written as

$$\mathbf{v}(\mathbf{x},t) = \sum_{n=1}^{\infty} a_n(t)\,\nabla\times(\mathbf{k}\,\psi_n(\mathbf{x})) + \sum_{n=1}^{\infty} b_n(t)\,\nabla\phi_n(\mathbf{x}) + \sum_{n=1}^{\infty} c_n(t)\,\nabla\phi_n^b(\mathbf{x}) .$$

[21] The equation above is the generalization of a Fourier transform for a velocity field defined on an arbitrary domain Ω. It has been useful in many applications because of two distinguished properties. First, every mode ψ_n, ϕ_n or ϕ_n^b satisfies the boundary condition, hence one can truncate the sequence at any n (e.g., for filtering) without altering the boundary conditions. The coefficients $a_n(t)$, $b_n(t)$, and $c_n(t)$ can also be modified (for example by numerical or experimental error) without any influence on the global boundary condition. Second, if the modes are ordered with respect to their eigenvalue λ_n, the length scales are approximately in decreasing order. This property is essential when one truncates the sequence as only the length scales above a certain threshold must be retained. It also permits to study energy at specific length scales.

[22] Using the above generalized Fourier modes, any bounded velocity field can, theoretically, be expanded using an infinite number of modes. In practice, the number of

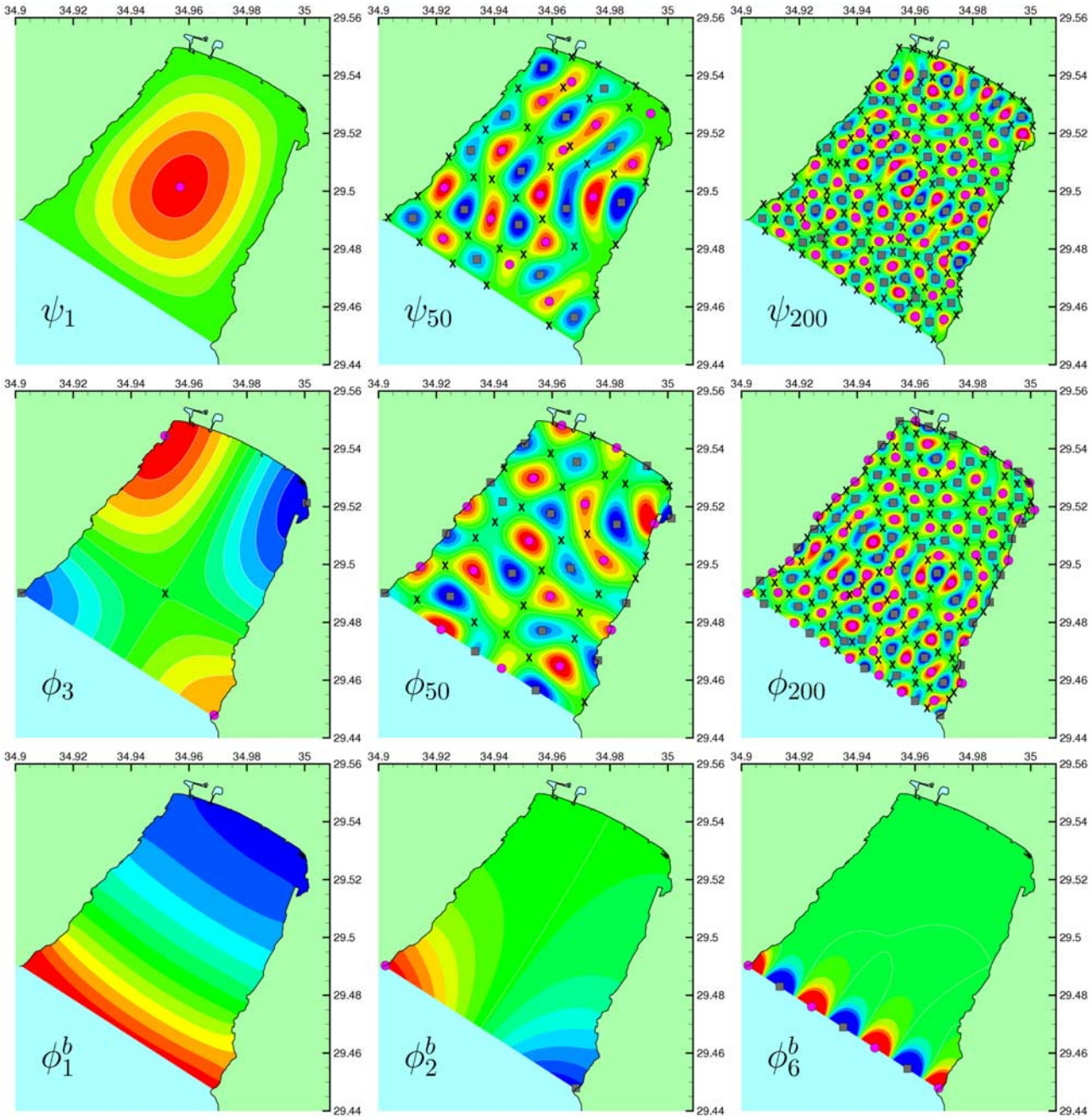

Figure 2. Selected (top) Dirichlet, (middle) Neumann, and (bottom) boundary modes for the Gulf of Eilat. Circles indicate clockwise vorticity centers (Dirichlet) or point sources (Neumann). Squares indicate counterclockwise centers (Dirichlet) or sinks (Neumann). Crosses indicate saddle points.

available modes is finite and only signals with wavelengths above a certain threshold are taken into account. One then has to decide what the threshold length scale is and how many modes are needed to represent the observed velocity field accurately. This the main subject of this manuscript.

3. Modal Length Scales

[23] In this section, we consider the open-boundary modes and present several approaches to define their synoptic length scale. We start from the well-known wavelength of Fourier modes in a rectangular basin. We then extend the definition to arbitrary OMA modes and we demonstrate the procedure in a nearly rectangular domain, which enables a clear comparison to the Fourier modes.

3.1. Length Scales of Fourier Modes

[24] Before defining and investigating the length scales of the generalized modes defined in the previous section, we briefly review Fourier modes and their length scales. Let us consider a rectangular box of length L and width W. Without

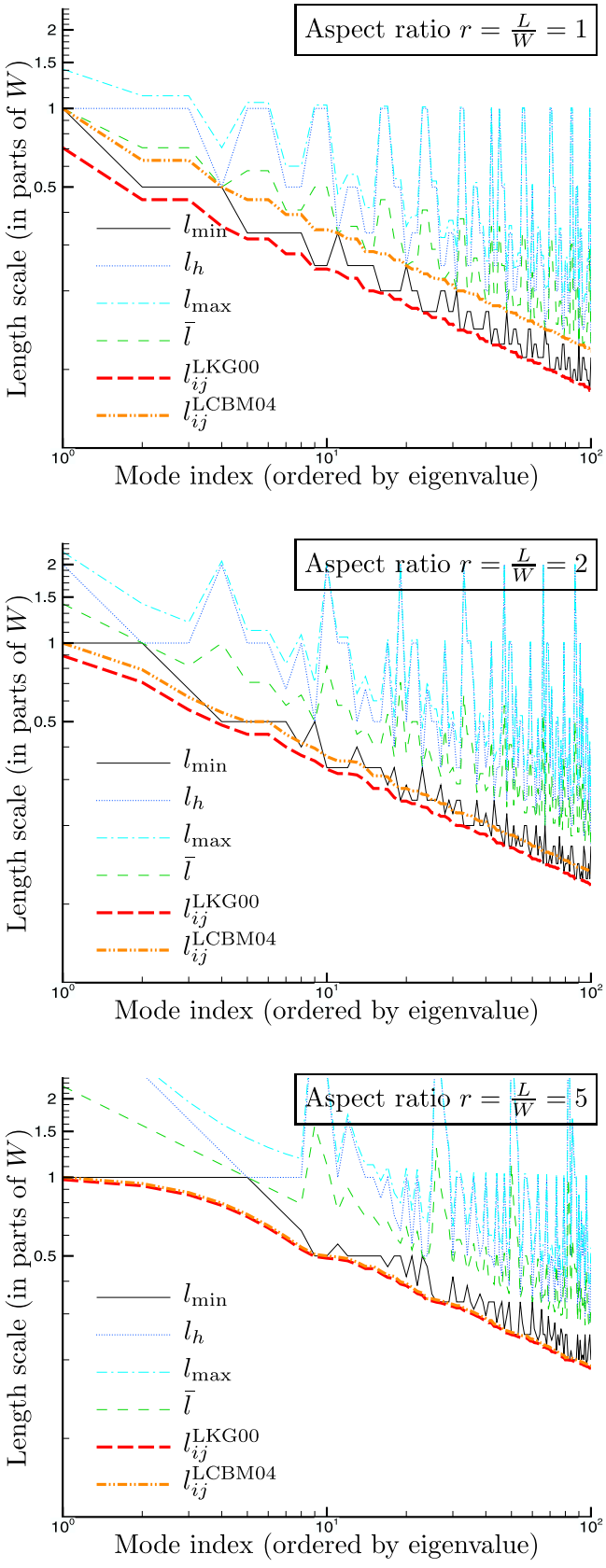

loss of generality, we assume $L \geq W$. The Fourier Dirichlet mode

$$\psi_{ij} = \sin\left(i\pi\frac{x}{L}\right)\,\sin\left(j\pi\frac{y}{W}\right),$$

delineates $N_c = ij$ identical eddy-like structures. We will refer to any large closed contour of the stream function as an eddy although it does not necessarily correspond to a real eddy in the current field. Rather than an actual physical process, the eddies in this manuscript represent the atomic features and, hence, the length scales of an observed mode.

[25] In the mode ψ_{ij}, the eddies are arranged in i columns and j rows. The length scale of the mode can be defined as the width (or smallest dimension) of the eddies: $l_{\min} \doteq \min\left\{\frac{L}{i}, \frac{W}{j}\right\}$. This is also the size of the smallest feature in the mode.

[26] One could also think about defining the length scale as the length (i.e., the largest dimension) of the eddies: $l_h \doteq \max\left\{\frac{L}{i}, \frac{W}{j}\right\}$ or the diameter of the eddies: $l_{\max} \doteq \sqrt{\frac{L^2}{i^2} + \frac{W^2}{j^2}}$ (i.e., the largest straight segment contained entirely in a single eddy). Nevertheless, as the arguments below show, only the width or (the size of the smallest feature) is acceptable and physically meaningful.

[27] 1. A basic requirement in defining modal length scales is the ability to order the modes. In particular, the set of modes whose length scale is smaller than a constant K must be finite and the number must be increasing with the constant K. To nowcast currents using OMA, one typically puts a threshold on the smallest length scale and projects the data on the modes whose length scales are larger than the threshold. This is only possible if there are only a finite number of modes whose length scale is smaller than the threshold. From this point of view, only $l_{\min}$ is a valid definition.

[28] 2. For a mode corresponding to $i = 1$ and $j = 1000$, we have $l_h = L$ and $l_{\max} \approx L$. One would, however, not attribute such a large length scale to this mode by looking at a plot of its level sets. Indeed, the mode contains very long but thin eddies whose widths are only $\frac{H}{1000} \ll L$. Only $l_{\min}$ is able to characterize this structure.

[29] 3. Two approximations of the length scale have been proposed in the literature. These approximations will be discussed in the next section, but we point out already that the approximation of *Lipphardt et al.* [2000], in the context of Fourier modes, states

$$l_{ij}^{\mathrm{LKG00}} = \frac{\pi}{\lambda_{ij}} = \frac{L\,W}{\sqrt{i^2W^2 + j^2L^2}}.$$

Figure 3. Length scale definitions for Fourier modes. l_h is the length or largest dimension of the eddies; $l_{\max}$ is the diameter of the eddies. These two definitions lead to a metric with which the modes cannot be ordered. $\bar{l}$ is the square root of the area per eddy and does not correspond to the actual length scale of the mode. $l_{\min}$ is the width of the eddies and a valid, ordering definition of the length scale. Previous length scale approximations [see *Lipphardt et al.*, 2000; *Lekien et al.*, 2004] bracket $l_{\min}$. Each panel corresponds to a different aspect ratio: (top) $r = L/W = 1$, (middle) $r = L/W = 2$, and (bottom) $r = L/W = 5$. Note that the number of modes below a specific threshold for definitions l_h, $l_{\max}$, and $\bar{l}$ is not necessarily finite.

The length scale approximation of *Lekien et al.* [2004] for Fourier modes gives

$$l_{ij}^{\mathrm{LCBM04}} = W\frac{\lambda_{11}}{\lambda_{ij}} = \frac{\sqrt{L^2+W^2}}{\sqrt{i^2W^2+j^2L^2}}.$$

[30] These approximations tell us how the length scale was defined in the context of operational modal reconstruction. Figure 3 shows the length scales $l_{\min}$, l_h, $l_{\max}$, and $\bar{l}$, as well as the approximations l_{ij}^{LKG00} and l_{ij}^{LCBM04}. The two approximations used previously bracket $l_{\min}$ and are not meant to represent the quantities $l_{\max}$ or l_h.

[31] Note that in this paper, the eigenvalues are written $-\lambda_{ij}^2$, and not just λ_{ij} as in the works by *Lipphardt et al.* [2000] and *Lekien et al.* [2004], hence the equations for the approximated length scales in these papers differ slightly from the equations above.

3.2. Length Scales of Dirichlet Eigenmodes

[32] We now turn to the generalized Fourier modes defined in section 2. The solution of $\Delta\psi_n = -\lambda_n^2\psi_n$ and $\psi_n = 0$ at the boundary, is a countable set of functions ψ_n (ordered by increasing eigenvalues λ_n). Although these modes reduce to the Fourier basis for a rectangular domain, the multiple index is irrelevant for a general domain Ω. This is the main difficulty in generalizing the length scale definition to the eigenfunctions: we do not have access to the exact distribution of the eddies in two independent directions (i and j). How can we generalize the definition of the length scale $l_{\min}$ to such modes?

[33] Let us consider the closed level sets of ψ_n. Courant's nodal line theorem states that there is, at most, n closed zero streamlines [*Courant and Hilbert*, 1953] and, hence, n eddy centers. Given the mode ψ_n, let us consider the N_c points $\mathbf{x}_k^c$ where ψ_n is a local extremum. Figure 2 shows the distribution of the centers $\mathbf{x}_k^c$ for selected modes. Numerically, we solve the eigenvalue problems using the finite element method and linear interpolation on the triangular elements. As a result, the numerical modes are piecewise linear and centers can be easily extracted [*Tricoche et al.*, 2000]. For each center $\mathbf{x}_k^c$, we consider the quantity

$$\min_{\substack{m=1\cdots N_c\\ m\neq k}} \left\{d\left(\mathbf{x}_k^c,\mathbf{x}_m^c\right)\right\},$$

where $d(\mathbf{x}_1, \mathbf{x}_2)$ is the distance between two points in the plane. This quantity gives the shortest distance between $\mathbf{x}_k^c$ and its neighbors. It is an approximation of the scale of the eddy of center $\mathbf{x}_k^c$. The only discrepancies arise near the boundary where the width might extend toward the boundary, i.e., in a direction where there are not any neighboring centers. For this reason, we define the generalized eddy width as

$$\mu_k = \min\left\{2\,d\left(\mathbf{x}_k^c,\partial\Omega\right), \min_{\substack{m=1\cdots N_c\\ m\neq k}}\left\{d\left(\mathbf{x}_k^c,\mathbf{x}_m^c\right)\right\}\right\}, \qquad (1)$$

where $d(\mathbf{x}_k^c, \partial\Omega)$ is the (shortest) distance between the center $\mathbf{x}_k^c$ and the boundary $\partial\Omega$.

[34] The quantities μ_k give a length scale for each eddy in the mode ψ_n. We assume that those length scales are similar for each eddy within a single mode but there are still several options for defining a single length scale from the N_c eddy length scales μ_k. We investigate the following candidates: (1) $L_{\min} = \min_{k=1\cdots N_c}\{\mu_k\}$, (2) $L_{\max} = \min_{k=1\cdots N_c}\{\mu_k\}$, (3) $L_{\mathrm{avg}} = \frac{1}{N_c}\sum_{k=1}^{N_c}\mu_k$, and (4) $L_{\mathrm{rms}} = \sqrt{\frac{1}{N_c}\sum_{k=1}^{N_c}\mu_k^2}$. Note that all the definitions above reduce to $l_{\min}$ when the domain is a rectangle (and for any aspect ratio). Do these length scales remain close for nonrectangular domains?

[35] Figure 4 also reveals that the gap between $L_{\min}$ and $L_{\max}$ vanishes quickly. Note that all the quantities plotted in Figure 4 behave asymptotically as $1/\sqrt{n}$, according to Weyl's law [*Weyl*, 1950; *Courant and Hilbert*, 1953]. Nevertheless, Figure 4 (bottom) also indicates that the relative difference between $L_{\max}$ and $L_{\min}$ remains above 30% as $n \to +\infty$. In other words, even for a very large mode index, the range of eddy length scales present in the mode remains finite. When a rectangular domain is even slightly perturbed (e.g., in the Gulf of Eilat), the generalized Fourier basis does not only bend the streamlines near the boundary and separate the degenerated eigenvalues. It also blurs the spectrum, and eddies with different length scales start coexisting within the same generalized mode.

[36] Which one of $L_{\min}$, L_{avg}, L_{rms}, and $L_{\max}$ should then be used to define the length scale of a mode?

[37] The analysis in the previous section shows that the width of an eddy, and not its diameter or its length, must be used to define the length scale of an eddy. Extrapolating this conclusion indicates that the smallest eddy length scale, $L_{\min}$, may be the most natural choice for the definition of the mode length scale. Indeed, thresholding the length scale in a modal decomposition process requires the ability to exclude modes that contain eddy length scale smaller than the threshold. Only $L_{\min}$ could fulfil this requirement.

[38] There are, however, two strong arguments against using $L_{\min}$ as a length scale definition. First, it is a rather noisy quantity and it is very sensitive to numerical errors. To derive the graph in Figure 4, the eigenmodes were computed on a mesh containing more than 100,000 triangular elements. Smaller meshes lead to similar eigenmodes but the extraction of the centers often leads to spurious or duplicate centers. Since $L_{\min}$ is given by the smallest eddy length scale, a duplicate center or a spurious center near the boundary can easily decrease $L_{\min}$ by several orders of magnitude. In Figure 4, the curves corresponding to $L_{\min}$ and $L_{\max}$ are much noisier and sensitive to perturbations than L_{avg} and L_{rms} which are averaged over all the eddies.

[39] The second argument against using $L_{\min}$ as the definition of the mode length scale is the fact that most eddies in a mode have a length scale much larger than $L_{\min}$. One of the eddies has a width $L_{\min}$ but most of them have scales closer to L_{avg}. This can already be deduced from Figure 4 which indicates clearly that $L_{\mathrm{avg}} \approx L_{\mathrm{rms}}$. It is easy

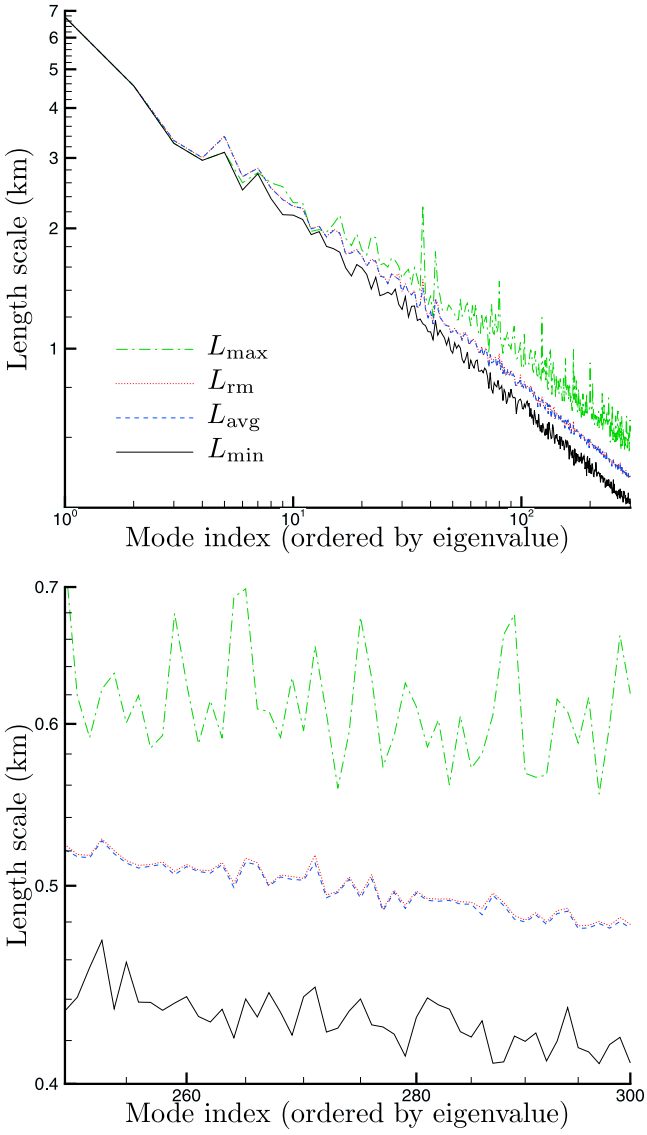

Figure 4. Comparison of candidate length scale definitions in the Gulf of Eilat. L_{min} and L_{max} are the length scale of the smallest and largest eddy, respectively. L_{avg} and L_{rms} are the average and the root means square of the eddy length scales for each mode.

to check from the definition that we must have $L_{rms} > L_{avg}$ and that the variance of the eddy length scale is given by

$$\sigma^2 = \frac{1}{N_c}\sum_{k=1}^{N_c}\left(\mu_k - L_{avg}\right)^2 = L_{rms}^2 - L_{avg}^2.$$

[40] In other words, the fact that $L_{rms} \approx L_{avg}$ implies that the variance σ^2 is small and that the length scales μ_k are clustered around their average L_{avg}. There are some eddies with a length scale close to L_{min} but the vast majority of the eddies in a mode have length scales close to $L_{avg} \approx L_{rms}$. Figure 5 gives the distribution of the eddy length scales μ_k for 3 different modes and corroborates the fact that $L_{avg} \approx L_{rms}$ usually gives a better representation of the mode length scale. We also note from Figure 5 that the upper end of the spectrum is very sparse and that the width of the largest eddy, L_{max}, is not a relevant length scale since only one, or very few, eddies are as broad as L_{max}.

[41] Since both L_{min} and $L_{avg} \approx L_{rms}$ are valid candidates for the definition of the mode length scale, we will study

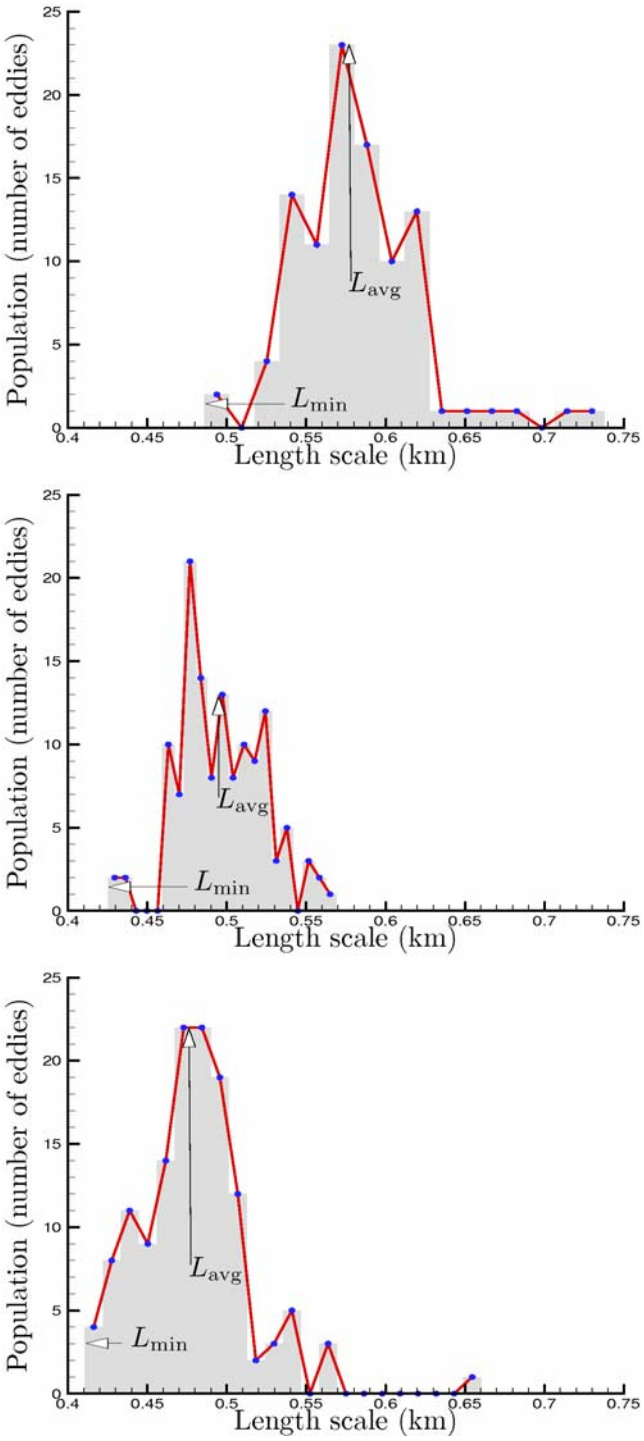

Figure 5. Distribution of the eddy length scale μ_k for Dirichlet modes (top) 200, (middle) 275, and (bottom) 300 in the Gulf of Eilat. L_{min} is the length scale of the smallest eddy but most of the eddies in a mode have a length scale close to $L_{avg} \approx L_{rms}$. Very few eddies have scales comparable to the maximum length scale L_{max}.

both quantities in the remaining of the manuscript. The various approximations will be compared to both $L_{\min}$ and L_{rms}. Note that the latter is so close to L_{avg} that a third comparison is obsolete.

3.3. Length Scale for Neumann Eigenmodes

[42] Although we have discussed the length scale of only Dirichlet Fourier modes in section 3.1, the results translate almost immediately to Neumann Fourier modes. Indeed, the length scale of

$$\psi_{ij} = \sin\left(i\pi\frac{x}{L}\right)\,\sin\left(j\pi\frac{y}{W}\right),$$

is the same as the length scale of

$$\phi_{ij} = \cos\left(i\pi\frac{x}{L}\right)\,\cos\left(j\pi\frac{y}{W}\right).$$

Following section 3.1, when $i \neq 0 \neq j$, the length scale of both Neumann and Dirichlet Fourier modes is given by

$$l_{\min} = \min\left\{\frac{L}{i}, \frac{W}{j}\right\}.$$

[43] The only difference between Neumann and Dirichlet modes is the domain of the indexes i and j. For Dirichlet modes, both i and j are strictly greater than 0. For Neumann modes, there are also nondegenerate solutions corresponding to either $i = 0$ or $j = 0$. Loosely speaking, for a given range of length scales, there are always more Neumann modes than Dirichlet modes. The length scale formula for Dirichlet Fourier modes does not accommodate for vanishing i and j, but we can generalize the formula as

$$l_{\min} = \begin{cases} \min\left\{\frac{L}{i}, \frac{W}{j}\right\} & \text{if } i > 0 \text{ and } j > 0\,, \\ \min\left\{L, \frac{W}{j}\right\} = \frac{W}{j} & \text{if } i = 0\,, \\ \min\left\{\frac{L}{i}, W\right\} & \text{if } j = 0\,. \end{cases}$$

The definition above is identical to that of Dirichlet Fourier modes, except for the modes corresponding to $i = 0$ and $j = 0$. When an index vanishes, we compute the length scale with the other index, but the result cannot exceed the spatial extent of the domain. Note that $L \geq W$, hence $L \geq \frac{W}{j}$.

[44] Let us now turn to Neumann modes on an arbitrary domain. The procedure depicted in section 3.2 for Dirichlet modes can be applied to Neumann modes. For Dirichlet modes, μ_k was, for each center $\mathbf{x}_k^c$, the smallest distance to another center (or twice the distance to the boundary, if smaller). For Neumann modes, we seek sinks and sources instead of centers. Unlike centers, some of these sources and sinks will be on the boundary. Taking this into consideration, we define the eddy length scale as

$$\mu_k = \min_{\substack{m-1\cdots N_c \\ m\neq k}} \left\{d\left(\mathbf{x}_k^c, \mathbf{x}_m^c\right)\right\},$$

where, for Neumann modes, N_c is the number of sources and sinks and $\mathbf{x}_k^c$ is the position of the kth point of divergence.

[45] Another approach consists of ignoring the sources and sinks that are on the boundary. In this case, the eddy length scale μ_k is given by the same formula as for Dirichlet modes (see equation (1)). Numerically, this can be implemented by ignoring sources and sinks that are within a small distance from the boundary. Note that this approach is consistent with the free-slip boundary condition which implicitly neglects the narrow boundary layer.

[46] Similarly, one can count the saddle points of the Neumann mode (instead of counting the sources and sinks) to determine the length scale (see Figure 2). Index theory [*Guckenheimer and Holmes*, 1983] guarantees that a saddle will be found in each closed loop made by the union of invariant lines between sources and sinks. Indeed, if we consider the velocity field $\nabla\phi$ where ϕ is a velocity potential mode, there are heteroclinic connections between sinks and sources. Any closed loop made by the union of heteroclinic connections can be deformed into a smooth loop that excludes the sinks and sources. The velocity vectors along the loop will rotate clockwise by 360° as the loop is traveled in a counterclockwise direction. As a result the loop has index -1 and it must contain at least one saddle point, which is the only fixed point associated with a negative index.

[47] If one counts the saddle points instead of the sources and sinks, the length scale is still given by equation (1) where N_c becomes the number of saddles and $\mathbf{x}_k^c$ are the positions of the saddles.

[48] Defining the length scale on the basis of the saddles in the Neumann modes results in a better mapping between Neumann and Dirichlet modes for a rectangular domain. Indeed the centers of

$$\psi_{ij} = \sin\left(i\pi\frac{x}{W}\right)\,\sin\left(j\pi\frac{y}{H}\right),$$

correspond exactly to the saddles of

$$\phi_{ij} = \cos\left(i\pi\frac{x}{W}\right)\,\cos\left(j\pi\frac{y}{H}\right).$$

[49] On nonrectangular domains, using the saddles of the Neumann modes to define their length scales guarantees also that there is no discrepancy between the length scale definitions for Neumann and Dirichlet modes. As an example, Figure 2 shows the modes ψ_1 and ϕ_3 which have the same length scale. The saddle in the Neumann mode plays the same role as the center in the Dirichlet mode. Index theory guarantees that except for the first few Neumann modes in which there might not be any source nor sink in the interior of the domain, the three approaches above yield similar results. We have implemented the three methods and found that after the 10th mode, they yield indistinguishable results. We note, however, that extracting saddle points is a more complicated numerical operation than the computation of sources and sinks (which are extrema of the velocity potential modes).

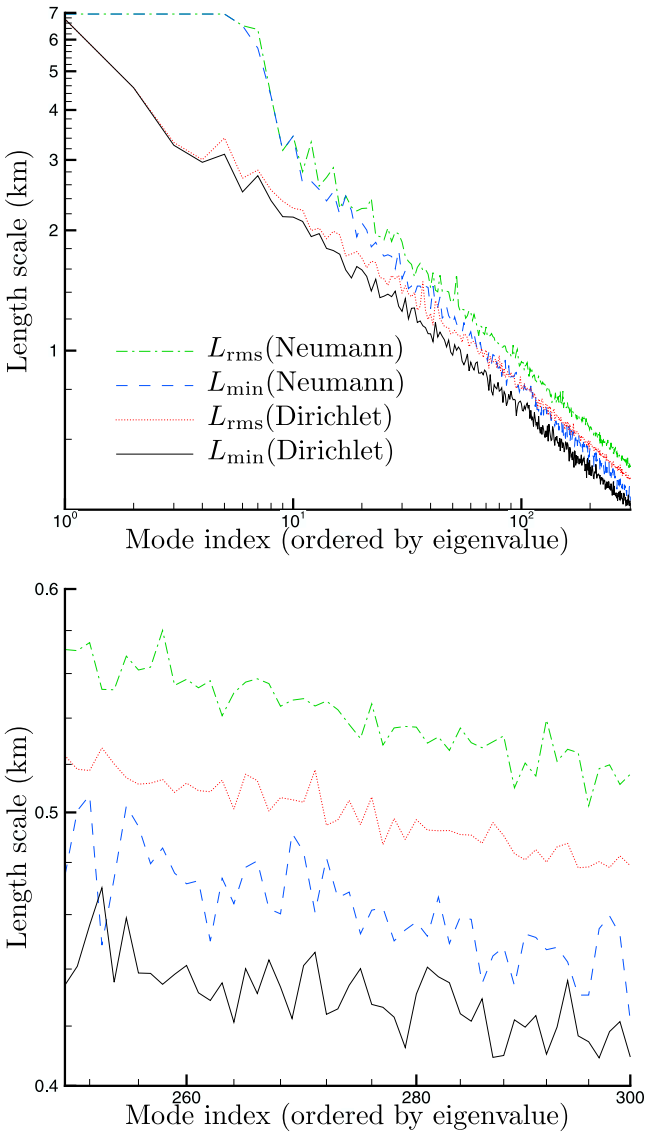

Figure 6. Comparison of the synoptic length scales for Dirichlet and Neumann modes in the Gulf of Eilat. $L_{\rm min}$ is the length scale of the smallest eddy. $L_{\rm rms}$ is the root mean square of the eddy length scales for each mode.

[50] Figure 6 compares the length scale of Neumann and Dirichlet modes. Both $L_{\rm min}$ and $L_{\rm rms}$ are investigated. As for Dirichlet modes, the ratio between $L_{\rm min}$ and $L_{\rm rms}$ remains uniformly bounded above 1. Depending on the application, one needs to select one of those two quantities as the reference. It is also worth noting that for a given index n, the length scale of the Neumann mode is always greater than the length scale of the Dirichlet mode. Indeed, for a given length scale threshold, there are always more Neumann modes with features larger than the threshold than there are Dirichlet modes. On a rectangle, these "extra" Neumann modes correspond to pairs of indexes (i, j) where either i or j vanishes.

[51] Also note that the differences between Neumann and Dirichlet modes vanish as the mode index, n, increases. Indeed, Figure 6 shows that the quantity $L_{\rm min}$ becomes the same for Neumann and Dirichlet modes as $n \to +\infty$. $L_{\rm rms}$ has the same asymptotic behavior.

3.4. Length Scale for Boundary Modes

[52] The boundary modes generate flux through segments the of open boundary [*Lekien et al.*, 2004]. They satisfy

$$\Delta\phi_n^b = \frac{\oint_{\partial\Omega} g_n(s)\,{\rm d}s}{{\rm Area}(\Omega)} \text{ inside } \Omega \quad \text{and} \quad \mathbf{n}\cdot\nabla\phi_n^b = g_n(s) \text{ on } \partial\Omega,$$

where $g_n(s)$ is a basis of functions on the open boundary (i.e., where the flux is nonzero). As in the works by *Lekien et al.* [2004] and *Kaplan and Lekien* [2007], we assume that a Fourier basis is used for g_n. For example, one can use

$$g_n(s) = \cos\left(\frac{n\pi s}{L_{\rm ob}}\right),$$

where $L_{\rm ob}$ is the length of the open boundary and $n \in \mathbb{N}$.

[53] As shown by *Lekien et al.* [2004] and by *Kaplan and Lekien* [2007], in this case, the length scale of the nth boundary mode is given by

$$L_n^{\rm ob} = \frac{L_{\rm ob}}{n+1}\ . \tag{2}$$

[54] Determining the length scale of the boundary modes is therefore a much simpler process than the corresponding operation for interior Dirichlet and Neumann modes. The formula above is exact and easily computed for any domain Ω. In comparison, the "synoptic length scales" $L_{\rm min}$ and $L_{\rm rms}$ for interior modes are much more difficult to compute as they require knowledge of the entire mode (as opposed to just the mode index, n, or the eigenvalue, λ) and the computation of centers or saddle points.

[55] In the next sections, we derive approximations for the length scale of the interior modes and we compare them to $L_{\rm min}$ and $L_{\rm rms}$. The objective is to find simple approximations that are readily computed (i.e., they depend only on n, λ, Area(Ω) and the aspect ratio r) for Dirichlet and Neumann modes. A similar analysis for boundary modes is unnecessary since equation (2) already provides the exact length scale in terms on n and $L_{\rm ob}$.

[56] Many approximated formulas for an arbitrary domain will require knowledge of an approximated length (largest dimension of the domain), an approximated width (smallest dimension of the domain) or the aspect ratio (ratio between length and width). In the next section, we derive a methodology for determining the width, length, and aspect ratio of an arbitrary domain.

4. Width and Length of an Arbitrary Domain

[57] To derive approximated formula for modal length scales, it is often convenient to start from a rectangular domain where the eigenvalues and the modes are known analytically. As a result, and as shown in the next sections, an approximation of the length L of the domain, its width W, or the aspect ratio $r = L/W$ are often needed to use these approximations. These are obvious for a rectangular domain.

However, how can we determine the "largest side" L and the aspect ratio of an arbitrary, nonrectangular domain Ω? In this section, we use the moment of inertia tensor of Ω to give a precise definition of L and W for an arbitrary domain.

4.1. Inertia Tensor

[58] If we consider a bounded open set $\Omega \subset \mathbb{R}^2$, its area is given by

$$\text{Area}(\Omega) = \iint_\Omega \mathrm{d}\mathbf{x} \,,$$

and the center of gravity of the domain is

$$\mathbf{x}_g = \frac{1}{\text{Area}(\Omega)} \iint_\Omega \mathbf{x}\, \mathrm{d}\mathbf{x} \,.$$

[59] Neither the area nor the center of gravity gives any information about the length and the width of the domain. The distribution of the domain about its center of gravity is determined by moments of inertia. Suppose that we pick a straight line in the plane that passes through the center of gravity of Ω. Such a line is defined by a unit vector $\boldsymbol{\omega}$ pointing in the direction of the axis. A measure of "how the domain is distributed about the axis" is given by the moment of inertia

$$\vec{\mathbf{i}}_\omega = \iint_\Omega \left(\mathbf{x} - \mathbf{x}_g\right) \times \left(\omega \times \left(\mathbf{x} - \mathbf{x}_g\right)\right) \mathrm{d}\mathbf{x}.$$

The moment of inertia can be computed for any axis $\boldsymbol{\omega} = (\omega_x, \omega_y)$ using the moment of inertia along the x and y axes:

$$\vec{\mathbf{i}}_\omega = \begin{pmatrix} \omega_x & \omega_y \end{pmatrix} \underbrace{\begin{pmatrix} I_{xx} & I_{xy} \\ I_{xy} & I_{yy} \end{pmatrix}}_{I} \begin{pmatrix} \omega_x \\ \omega_y \end{pmatrix},$$

where $I_{xx} = \mathbf{1}_x \cdot \vec{\mathbf{i}}_x$ is the x component of the moment of inertia with respect to the x axis, and $I_{xy} = \mathbf{1}_y \cdot \vec{\mathbf{i}}_x$ is the y component of the moment of inertia with respect to the x axis.

[60] By definition, we have $I_{xy} = I_{yx}$, hence the 2×2 inertia tensor is symmetric. As a result, the matrix I has two real eigenvalues corresponding to two orthogonal eigenvectors. The norm of the moment of inertia, $\|\vec{\mathbf{i}}_\omega\|$ gives a measure of "how far the domain extends in the direction perpendicular to $\boldsymbol{\omega}$." The direction $\boldsymbol{\omega}$ is parallel to "the largest side" of the domain if $\|\vec{\mathbf{i}}_\omega\|$ is a minimum. The direction $\boldsymbol{\omega}$ is parallel to "the smallest side" of the domain if $\|\vec{\mathbf{i}}_\omega\|$ is maximum. In other words, the distribution of the domain can be represented by a rectangle whose sides are parallel to the (orthogonal) eigenvectors of the inertia tensor. The eigenvalues of the inertia tensor give the length of the sides of the rectangle.

4.2. Length and Width of Ω

[61] The inertia tensor gives us a way to compute a rectangle that fits the mass distribution inside an arbitrary domain Ω. The real eigenvalues $\lambda_{\max}$ and $\lambda_{\min}$ encode information about the size of this rectangle. To extract the length and width, we seek a rectangle that has an inertia tensor identical to the original domain Ω. Using a rotation matrix R that maps the coordinates in the reference frame of the eigenvectors of the inertia tensor, we rewrite the inertia tensor as

$$I = R \begin{pmatrix} \lambda_{\max} & 0 \\ 0 & \lambda_{\min} \end{pmatrix} R^\top.$$

[62] The inertia tensor of a rectangle whose sides are L and W and are aligned with the same eigenvectors is given by

$$I = \frac{1}{3} R \begin{pmatrix} L^3 W & 0 \\ 0 & L W^3 \end{pmatrix} R^\top.$$

We require that the rectangle used to approximate the domain has the same area as the original domain Ω, hence $\text{Area}(\Omega) = LW$ and we rewrite the equation above as

$$I = \frac{\text{Area}(\Omega)}{3} R \begin{pmatrix} L^2 & 0 \\ 0 & W^2 \end{pmatrix} R^\top.$$

For the inertia tensor of the domain Ω to match that of the approximating rectangle, we need to set

$$\begin{aligned} L &\doteq \sqrt{\frac{3\lambda_{\max}}{\text{Area}(\Omega)}}, \\ W &\doteq \sqrt{\frac{3\lambda_{\min}}{\text{Area}(\Omega)}}. \end{aligned}$$

[63] The formula above gives the length and width of the rectangle that has the same center of gravity, the same area, and the same moment of inertia as the domain of interest, Ω. Given Ω, it provides a way to compute the length and width directly using the eigenvalues of the moment of inertia tensor. The orientation of the rectangle is given by the eigenvectors of the tensor.

[64] It is worth noting that computing the eigenvectors becomes a singular problem when the eigenvalues are identical or very close to each other (i.e., when the aspect ratio of the domain is close to 1). The largest eigenvalue, which gives the "largest side of the domain" is, however, continuous, independently of the aspect ratio of the domain. In other words, it might be difficult to plot the actual approximating rectangle when the aspect ratio is close to 1, but determining the largest length scale of the domain and its aspect ratio is never a singular problem [*Dieci and Eirola*, 1999].

4.3. Examples

[65] Figure 7 shows the results of two numerical applications: the nearly rectangular basin of the Gulf of Eilat (that we study in this manuscript) and Monterey Bay which has a more complex coastline [see, e.g., *Paduan and Rosenfeld*, 1996]. The surface currents in these two regions are sampled using coastal radar stations. For using some of the approximated length scale formula derived in the next sections and selecting the number of OMA modes to use, one needs to evaluate the "largest side" and the "smallest

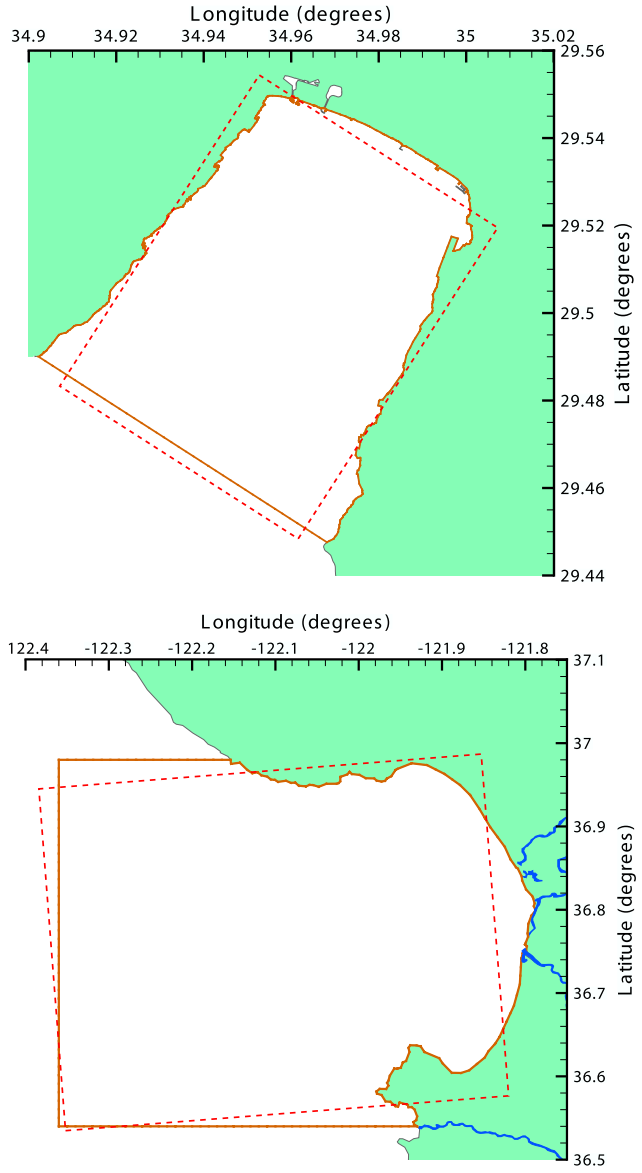

Figure 7. Computation of the width and length for the HF radar covered regions in (top) the Gulf of Eilat and (bottom) Monterey Bay. The solid line indicates the computational domain where modes and nowcasts are computed. The dashed line is the rectangle built on the inertia tensor of the domains that provides width and length for each domain.

side" of these domains. According to the method described above, these lengths are $(L, W) = (8.17 \text{ km}, 6.26 \text{ km})$ for the Gulf of Eilat, and $(L, W) = (47.6 \text{ km}, 36.7 \text{ km})$ for Monterey Bay. Figure 7 also shows the corresponding approximated rectangles (dashed rectangles). On both panels, a thick line indicates the boundary of a computational domain Ω where enough data is available for modal analysis. OMA modes and nowcasts are computed for these domains.

5. Approximated Length Scales

[66] Both the smallest eddy width ($L_{\min}$) and the average eddy width (L_{rms}) are acceptable definitions for the mode length scale. These quantities are, however, difficult to compute since they require intensive and subtle computations to extract centers and saddles. In this section, we investigate several approximations of the length scale and compare them to $L_{\min}$ and L_{rms}.

5.1. A Lower Bound: L^{LKG00}

[67] Let us consider a rectangle and the corresponding Fourier eigenvalues

$$\lambda_{ij}^2 = \pi^2 \left(\frac{i^2}{L^2} + \frac{j^2}{W^2} \right). \tag{3}$$

For a given λ, there might be several couples (i, j) satisfying the equation above but we always have

$$1 \le i \le L \sqrt{\frac{\lambda^2}{\pi^2} - \frac{j^2}{W^2}} < L \frac{\lambda}{\pi}, \tag{4}$$

and

$$1 \le j \le W \sqrt{\frac{\lambda^2}{\pi^2} - \frac{i^2}{L^2}} < W \frac{\lambda}{\pi}. \tag{5}$$

The length scale of a Fourier mode is given by

$$L_{\min} = \min \left\{ \frac{L}{i}, \frac{W}{j} \right\},$$

hence we need to treat the couples (i, j) differently on the basis of the relative magnitude of L/i and W/j. From equation (3), we deduce that $L/i \le W/j$ if and only if

$$i \ge \frac{\lambda L}{\sqrt{2}\,\pi}.$$

In this case, we have

$$L_{\min} = \frac{L}{i} > \frac{\pi}{\lambda},$$

where we have used the last inequality in (4).

[68] Similarly, when $L/i > W/j$, we find

$$j > \frac{\lambda W}{\sqrt{2}\,\pi},$$

and

$$L_{\min} = \frac{W}{j} > \frac{\pi}{\lambda},$$

by the last inequality in (5).

[69] In other words, we have shown that π/λ is always strictly smaller than $L_{\min}$ for a Dirichlet mode on a rectangle. This lower bound was used as an approximation of the length scale used by *Lipphardt et al.* [2000], hence we define

$$L^{\text{LKG00}} \doteq \frac{\pi}{\lambda},$$

as a first candidate approximation of $L_{\min}$.

[70] Note that the lower bound is valid for any rectangle; it does not depend on the aspect ratio $r = L/W$. In general, L^{LKG00} does not need to remain a lower bound of $L_{\min}$ when the domain is not a rectangle. Nevertheless, as demonstrated in the next section, we expect this quantity to provides an approximate lower bound of the length scale.

[71] The lower bound L^{LKG00} is valid for both Dirichlet and Neumann modes. In the case of a Neumann mode, however, the last inequalities in equations (4) and (5) are not strict and the lower bound is not strict. For some Neumann modes, $L_{\min}$ becomes equal to the lower bound L^{LKG00}.

5.2. An Upper Bound: L^{up}

[72] We have established that when $L/i \leq W/j$, we have $i \geq \frac{\lambda L}{\sqrt{2}\pi}$. In this case,

$$L_{\min} = \frac{L}{i} \leq \sqrt{2}\,\frac{\pi}{\lambda}.$$

When $L/i > W/j$, we have $j > \frac{\lambda W}{\sqrt{2}\pi}$ and

$$L_{\min} = \frac{H}{j} \leq \sqrt{2}\,\frac{\pi}{\lambda}.$$

In both cases, and for any rectangle, we have the upper bound

$$L_{\min} \leq \sqrt{2}\,\frac{\pi}{\lambda} \doteq L^{\mathrm{up}}.$$

[73] The upper bound L^{up} is only valid for a rectangular domain, but we also expect it to overestimate the length scale of a mode for a nonrectangular region. Note that contrary to the lower bound L^{LKG00}, the upper bound is not strict. For any rectangle, an infinite number of modes have a length scale equal to L^{up}.

[74] Note that *Lipphardt et al.* [2006] use the length scale formula $\frac{2\pi}{\lambda}$ instead of the formula $L^{\mathrm{LKG00}} = \frac{\pi}{\lambda}$ from previous work [*Lipphardt et al.*, 2000]. The quantity $\frac{2\pi}{\lambda}$ is always greater than the upper bound $L^{\mathrm{up}} = \sqrt{2}\,\frac{\pi}{\lambda}$ and is not a good approximation of the mode length scale in the sense developed here. All the formulas and definition in this manuscript attempt to define the eddy diameter, or half the wavelength of the modes. Indeed, a full period of an oscillating mode has both a minimum and a maximum, hence two eddies. The formulas used by *Lipphardt et al.* [2006] describe the full wavelength of the modes and, hence, translate into $\frac{\pi}{\lambda}$ in the context of this study. Similarly, any definition and formulas from this manuscript can be multiplied by two to obtain results in terms of full wavelengths.

5.3. A Dimensional Approximation: L^{LCBM04}

[75] In the work by *Lekien et al.* [2004], an approximation of the modal length scale is derived on the basis of Buckingham's Π theorem [*Buckingham*, 1914; *Curtis et al.*, 1982]. If nothing but the eigenvalue $(-\lambda_n^2)$ is known, Buckingham's dimensional analysis provides a strong constraint on the relationship between λ_n and the length scale, L_n, of the nth mode: their product is a constant that does not depend on the mode index n. We can therefore find the length scale of any mode on the basis of a reference mode as follows

$$L_n = L_{\mathrm{ref}}\,\frac{\lambda_{\mathrm{ref}}}{\lambda_n},$$

[76] For Dirichlet modes, the reference is naturally the first mode [*Lekien et al.*, 2004; *Kaplan and Lekien*, 2007]. Indeed, the first mode corresponds to a single gyre with length scale $L_1 = W$ (e.g., for a rectangle, $\psi_{11} = \sin(\pi x/L)\sin(\pi y/W)$). As a result, on the basis of Buckingham's Π theorem, the length scale of any Dirichlet mode is approximated by

$$L_n = W\,\frac{\lambda_1}{\lambda_n},$$

which is the result given by *Lekien et al.* [2004].

[77] For Neumann modes, using the same formula usually underestimates the length scale [*Kaplan and Lekien*, 2007]. This is a consequence of the fact that the reference Dirichlet mode does not correspond to the first Neumann mode. For a rectangle, the first Dirichlet mode is ψ_{11}. The corresponding Neumann mode (with the same length scale W) is ϕ_{11} but it is not the first Neumann mode. At least ϕ_{01} and ϕ_{10} have smaller eigenvalues than ϕ_{11}.

[78] We can therefore apply Buckingham's Π theorem also to Neumann modes, provided that we use the correct reference ϕ_{11}. Let us denote by μ the index of ϕ_{11} in the list of Neumann modes ordered by eigenvalues. The length scale of the nth Neumann mode is then given by

$$L_n = W\frac{\lambda_\mu}{\lambda_n}.$$

[79] The formula above is not very useful since the index μ of the reference mode is usually unknown. For a square ($L = W$), there are only 2 modes with eigenvalues smaller than that of ϕ_{11}, hence $\mu = 3$. When the aspect ratio $r = L/W > 1$, the reference index can be larger than 3. For the Gulf of Eilat ($r \approx 1.3$), Figure 2 shows that we have $\mu = 3$: the third Neumann mode has the same length scale as the first Dirichlet mode.

[80] Fortunately, one does not need to compute the exact index μ to evaluate the eigenvalue λ_μ and use the formula above. Indeed, on a rectangle, we have

$$\lambda_\mu^2 = \lambda_{11}^2 = \pi^2\left(\frac{1}{L^2} + \frac{1}{W^2}\right).$$

Since we assume $L \geq W$, the smallest eigenvalue λ_1 is given by

$$\lambda_1^2 = \frac{\pi^2}{L^2},$$

hence the approximated Neumann length scale can be rewritten

$$L_n = W\frac{\lambda_\mu}{\lambda_1}\frac{\lambda_1}{\lambda_n} = W\sqrt{1+r^2}\,\frac{\lambda_1}{\lambda_n},$$

where $r = L/W$ is the aspect ratio.
The dimensional approximation can then be summarized as

$$L^{\mathrm{LCBM04}} = \nu W \frac{\lambda_1}{\lambda}, \tag{6}$$

where $\nu = 1$ for Dirichlet modes and $\nu = \sqrt{1+r^2}$ for Neumann modes.

5.4. An Exact Formula for Fourier Modes: L^{rect}

[81] For Fourier modes, the number of centers (or saddles) inside the domain is given by

$$N_c = ij.$$

Since equation (3) gives another equality involving i and j, it is possible to determine i and j from λ and N_c. We have

$$\begin{cases} i = \sqrt{\dfrac{L^2\lambda^4}{2\pi^2} \pm \dfrac{L^2}{2}\sqrt{\dfrac{\lambda^2}{\pi^4} - 4\dfrac{N_c^2}{W^2L^2}}}, \\ j = \sqrt{\dfrac{W^2\lambda^4}{2\pi^2} \mp \dfrac{W^2}{2}\sqrt{\dfrac{\lambda^2}{\pi^4} - 4\dfrac{N_c^2}{W^2L^2}}}. \end{cases}$$

As a result, we get

$$L_{\min} = \min\left\{\frac{L}{i}, \frac{W}{j}\right\} = \sqrt{2}\,\frac{\pi}{\lambda}\left(1 + \sqrt{1 - \frac{4\pi^4 N_c^2}{\lambda^4 W^2 L^2}}\right)^{-\frac{1}{2}}.$$

The formula above gives the exact length scale $L_{\min}$ for any Fourier mode as a function of its eigenvalue λ, the number of eddy centers N_c, and the area of the domain $\mathrm{Area}(\Omega) = LW$. The formula is only exact for rectangular domains but, for arbitrary regions, we define the candidate approximation

$$L^{\mathrm{rect}} \doteq \sqrt{2}\,\frac{\pi}{\lambda}\left(1 + \sqrt{1 - \frac{4\pi^4 N_c^2}{\lambda^4 \mathrm{Area}^2(\Omega)}}\right)^{-\frac{1}{2}}. \tag{7}$$

Note that for Neumann modes, N_c is the number of saddle points, not the number of centers.

5.5. Variants of L^{rect}

[82] Equation (7) gives the exact length scale when the domain is a rectangle and is expected to perform very well on other domains. It does, however, require the computation of N_c, the number of centers (or saddles for Neumann modes). Since N_c is difficult to compute and is subject to a high numerical error, it is often preferable to approximate N_c using the eigenvalue λ or the mode index n. We note the following distinguished values for N_c:

[83] 1. The first value is $N_c^{\max}$. On a rectangle, we have

$$j^2 = W^2\left(\frac{\lambda^2}{\pi^2} - \frac{i^2}{L^2}\right),$$

hence,

$$N_c^2 = i^2 j^2 = W^2\left(i^2\frac{\lambda^2}{\pi^2} - \frac{i^4}{L^2}\right),$$

which is maximum when $i = \frac{\lambda W}{\sqrt{2}\pi}$. As a result, for a given eigenvalue λ, the maximum value of N_c is

$$N_c^{\max} = \frac{\lambda^2\,\mathrm{Area}(\Omega)}{2\pi^2}.$$

Substituting the expression above in equation (7), we find

$$L_{\max}^{\mathrm{rect}} \doteq \sqrt{2}\,\frac{\pi}{\lambda},$$

which is identical to the upper bound L^{up}.

[84] 2. Similarly, one can determine that the minimum value for N_c is $N_c^{\min} = \lambda H/\pi$. As a result, we have

$$L_{\min}^{\mathrm{rect}} = \sqrt{2}\,\frac{\pi}{\lambda}\left(1 + \sqrt{1 - \frac{4\pi^2}{\lambda^2 r\,\mathrm{Area}(\Omega)}}\right)^{-\frac{1}{2}}.$$

The expression above becomes asymptotically (i.e., for $\lambda \to +\infty$) identical to the lower bound L^{LKG00} but improves the estimate for eigenmodes corresponding to small eigenvalues.

[85] 3. Since we have both the minimum and maximum value for N_c, we can also use the average

$$N_c^{\mathrm{avg}} = \frac{N_c^{\max} + N_c^{\min}}{2} = \frac{\lambda^2\mathrm{Area}(\Omega)}{4\pi^2} + \frac{\lambda W}{2\pi}.$$

Substitution in equation (7) gives

$$L_{\mathrm{avg}}^{\mathrm{rect}} \doteq \frac{\pi}{\lambda}\,\frac{2}{\sqrt{2 + \sqrt{3 - 4\frac{\pi^2}{\lambda^2 r\,\mathrm{Area}(\Omega)} - 4\frac{\pi}{\lambda\sqrt{r\,\mathrm{Area}(\Omega)}}}}}.$$

Notice that as $\lambda \to +\infty$, we have

$$L_{\mathrm{avg}}^{\mathrm{rect}} \to \frac{2}{\sqrt{2+\sqrt{3}}}\,\frac{\pi}{\lambda} \approx 1.035\,\frac{\pi}{\lambda},$$

which is almost identical to L^{LKG00}. As a result, the approximation $L_{\mathrm{avg}}^{\mathrm{rect}}$ is, asymptotically, very similar to the lower bound L^{LKG00}, but it provides a better estimate for low eigenvalues for which the lower bound L^{LKG00} is usually too conservative.

[86] 4. Another estimate for N_c can be obtained by "counting" the modes for which the number of centers is smaller than N_c. Recall that we have $1 \le i \le N_c + 1$, and the number of modes, n, which have less than N_c centers is approximately equal to the area under the curve N_c/i in the (i, j) plane. This gives

$$n \approx \int_1^{N_c+1} \frac{N_c}{i}\,\mathrm{d}i = N_c\,\ln(N_c+1).$$

One can check that the function $x\,\ln(x+1)$ is strictly increasing for positive x. As a result, one can compute its inverse,

$$N_c = \gamma(n),$$

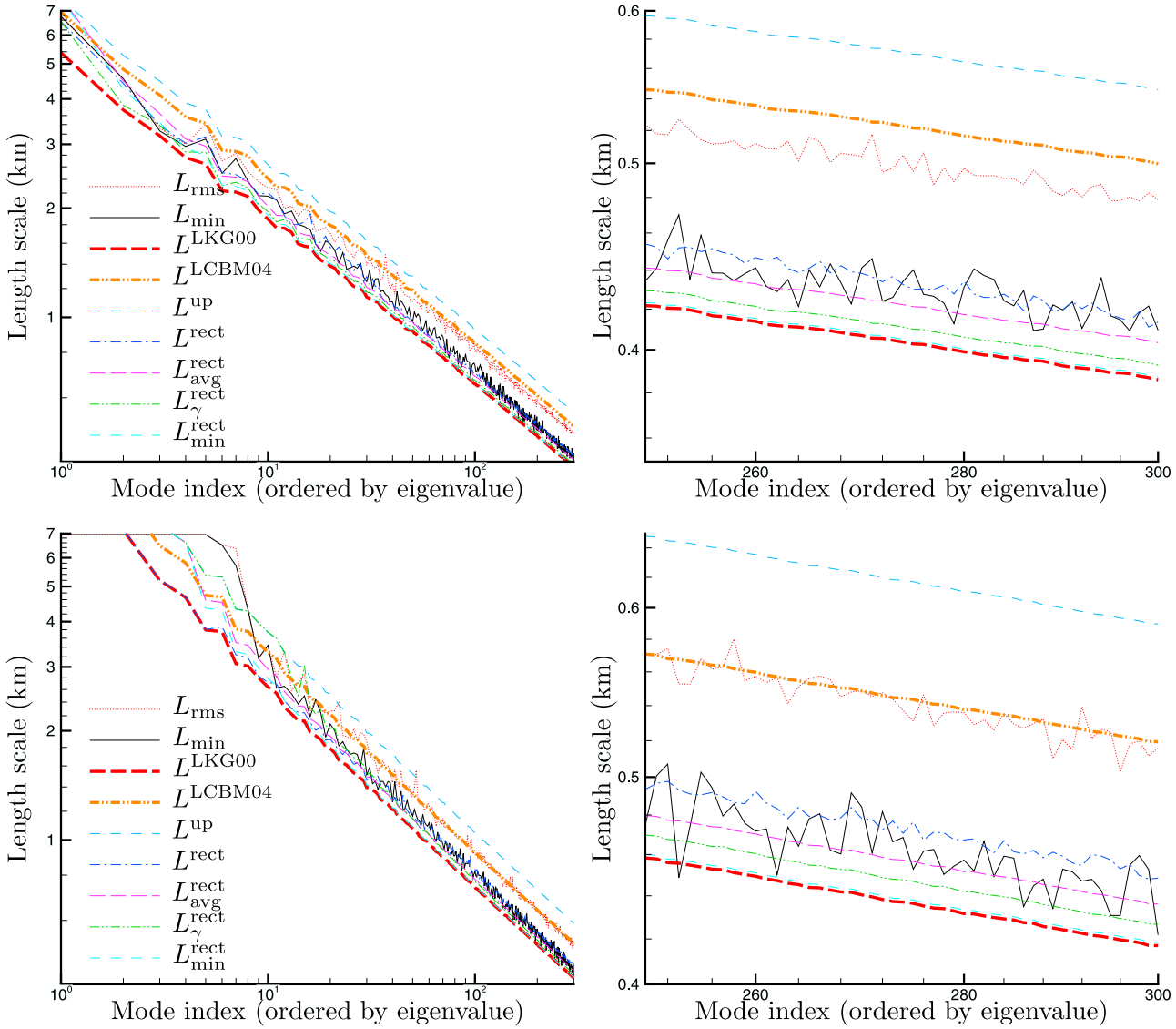

Figure 8. Comparison of the synoptic length scales for (top) Dirichlet and (bottom) Neumann modes in the Gulf of Eilat. L_{min} is the length scale of the smallest eddy. L_{rms} is the root means square of the eddy length scales for each mode. Both L_{min} and L_{rms} can be considered as a synoptic length scale and we seek their best approximation.

which gives the number of centers (or saddles) as a function of the mode index n. Notice that the inverse of $x \ln(x+1)$ does not have an analytic expression, hence one needs to evaluate γ numerically or build a seek table. Given the mode index n, we can then approximate N_c using the tabulated function γ, and the expression

$$L^{\mathrm{rect}}_{\gamma} \doteq \sqrt{2}\,\frac{\pi}{\lambda}\left(1+\sqrt{1-\frac{4\pi^4\gamma^2(n)}{\lambda^4\,\mathrm{Area}^2(\Omega)}}\right)^{-\frac{1}{2}}$$

is an estimate of the length scale of the mode.

[87] At first, one would expect the approximation above to yield poor results as the argument used to derive it is flawed: we have computed the number of modes which have less than N_c centers, but this quantity cannot be easily related to the mode index n. Indeed, the mode index n depends on the position of the mode in a sequence that has been ordered by length scale or by eigenvalue. However, the computation above assumes that the index n gives the position in a sequence ordered by N_c. There is no guarantee that the ordering by eigenvalue is even close to the ordering by number of centers. In fact, for rectangular domains, one can show that the two orderings (and the two definitions of the mode index n) are very different.

[88] As a result, when one evaluates N_c as $\gamma(n)$ where n is the actual mode index (i.e., ordered by eigenvalue), the error can be quite large. Nevertheless, the next section will reveal that only $L^{\mathrm{rect}}_{\mathrm{avg}}$ outperforms $L^{\mathrm{rect}}_{\gamma}$. We cannot fully explain this result but, intuitively, the reason is that in a non-rectangular domain, the eigenmodes rearrange in such a way that long eddies are replaced by (more numerous) isotropic eddies. Provided that the boundary of the domain is complex enough, most modes tend to be uniformly

distributed [*Shnirelman*, 1974]. For example, on a square, the modes $(i, j) = (100, 1)$ and $(i, j) = (1, 100)$ corresponds to $N_c = 100$, a relatively small number of centers for a large eigenvalue. The configurations with thin eddies are, however, unstable and any perturbation of the domain will modify the pair immediately in such a way that the number of centers is higher in the perturbed modes (see, e.g., *Trefethen and Betcke* [2006, Figure 5] for an illustration of this process on a square with a snipped corner).

[89] The accuracy of L_γ^{rect} is therefore not a consequence of its accuracy for a rectangular domain. It is, in fact less accurate than the other approximations for a rectangle. Instead, its strength comes from its ability to model a complex phenomena that takes place when one deforms a rectangular domain into a complex domain Ω: the mode index with respect to N_c becomes more and more similar to the mode index with respect to λ as the domain Ω looks less and less like a rectangle.

6. Comparison

[90] Figure 8 shows $L_{\min}$ and L_{rms} for Dirichlet and Neumann modes in the Gulf of Eilat. Recall that depending on the application, either $L_{\min}$ or L_{rms} could be selected as the "true synoptic length scale." Superimposed on each of these plots are the approximations developed in the previous section.

[91] We draw the following conclusions:

[92] 1. If one uses the average eddy width L_{rms} as the true length scale, then the best approximation is L^{LCBM04}. It is worth noting that this conclusion only holds for domains whose aspect ratio is close to 1.5. For the Gulf of Eilat, the tensor of inertia reveals that the aspect ratio $r \approx 1.3$ and L^{LCBM04} performs well. Inspecting Figure 3 reveals that L^{LCBM04} is no longer the best approximation of L_{rms} when $r \approx 1$ or $r > 2$. For $r \approx 1$, L^{LCBM04} overestimates the length scale. For $r > 2$, L^{LCBM04} tends to L^{LKG00}, which underestimates the length scale. None of our approximations are, however, close to L_{rms} for $r > 2$. $L_{\text{avg}}^{\text{rect}}$ is the closest but there is a significant error. In these cases, we suggest to use the average between the upper and lower bounds: $1/2\,(L^{\text{up}} + L_{\min}^{\text{rect}})$.

[93] 2. If one uses the smallest eddy length scale $L_{\min}$ as the truth, then the best approximation is L^{rect}, which requires counting the exact number of centers (or saddle points for Neumann modes).

[94] 3. If one uses the smallest eddy length scale $L_{\min}$ as the truth and does not want to extract features such as centers and saddle points, then the best approximation is $L_{\text{avg}}^{\text{rect}}$.

[95] 4. If one is interested in a lower bound of the minimum length scale $L_{\min}$, the approximation L^{LKG00} is rather conservative (both asymptotically and for small eigenvalues). At almost no extra computational cost, L_γ^{rect} and $L_{\min}^{\text{rect}}$ provide much better lower bounds on $L_{\min}$.

[96] It is worth noting that *Lipphardt et al.* [2006] used the approximation $L^{\text{LSK06}} = \frac{2\pi}{\lambda}$ which is twice the lower bound $L^{\text{LKG00}} = \frac{\pi}{\lambda}$. Since $L^{\text{LSK06}} = \frac{2\pi}{\lambda} > \sqrt{2}\,\frac{\pi}{\lambda} = L^{\text{up}}$, the quantity L^{LSK06} overestimates the length scale. Figure 8 confirms that L^{LSK06} is not a good approximation of the length scale (in the context of this manuscript). The formula $L^{\text{LSK06}} = \frac{2\pi}{\lambda}$ should be seen as a lower bound for the full oscillation wavelength (double the eddy length scale). It is equal to two twice L^{LKG00} and should be compared to the double of the quantities in this manuscript.

[97] Note also that the formulas L^{LKG00}, L^{LSK06} and L^{up} have, however, an invaluable advantage: they depend only on the eigenvalue λ, which is readily available from the mode solver. All the other formulas require the computation of the area of the domain, the width W, the aspect ratio r or other less trivial quantities.

7. Nowcasting in the Gulf of Eilat

[98] The northern tip of the Gulf of Eilat is a nearly rectangular, deep, and semienclosed basin in the northeast region of the Red Sea. Two 42 MHz HF radar (SeaSonde) stations are installed on the western coast of the gulf, one at the InterUniversity Institute and the other at the Port of Eilat (separated by approximately 5 km). This network enables observing the 6 km $\times$ 10 km region at a spatial resolution of about 300 m and a temporal resolution of 30 minutes (see Figure 1). More details on the deployment and validation of this network are given by *Gildor et al.* [2009].

[99] To proceed with OMA nowcasting, we begin by plotting the length scale as a function of the mode index for Dirichlet, Neumann, and boundary modes in Figure 9. Using this plot, we can determine the number of modes needed on the basis of the desired resolution. On the basis of Nyquist criterion, the smallest mode must be larger or equal to the spatial resolution of the data to avoid aliasing. (Note that Nyquist criterion states that the sampling frequency must be at least twice the frequency of the signal. In our case, however, the mode length scale is half the wavelength, hence the factor 2 disappears from the criterion.) One must, however, also ensure that the number of modes used does not exceed the number of radial currents available. This second requirement is usually more constraining than Nyquist criterion. For the Gulf of Eilat, it is typically possible to assimilate radial data down to a 350 m resolution. Wherever we have two nearby radial measurements, we can directly recombine the radial data into total vectors [*Barrick*, 2002]. The resulting total vectors count for two radial measurements and can also be assimilated using the OMA modes. In this case, however, fewer modes can be used since some unpaired radial currents have been discarded. It is typically possible to assimilate total currents down to a 400 m resolution in the gulf. Because there are many more radials than totals, it is therefore more advantageous to do the OMA nowcasts using radial data [*Kaplan and Lekien*, 2007]. Another advantage of this procedure is that it circumvents the errors that result from the way radials are combined into totals, specifically the Geometric Dilution Of Precision (GDOP [*Barrick*, 2002; *Kim et al.*, 2008]). Using the radials, we avoid the errors in totals and we use more data. Note that as a result, the OMA analysis which assimilates radial data can also be seen as another way to combine radials into totals. Recently, *Kim et al.* [2008] presented a generalized optimal interpolation method to compute surface currents from radials.

[100] We selected 4 different resolution lengths (400 m, 600 m, 1 km, and 2 km) and, using the curves shown in Figure 9, we determined the number of Dirichlet, Neumann, and boundary modes for each case (Table 1). It is worth noting that the plot in Figure 9 can be easily checked or

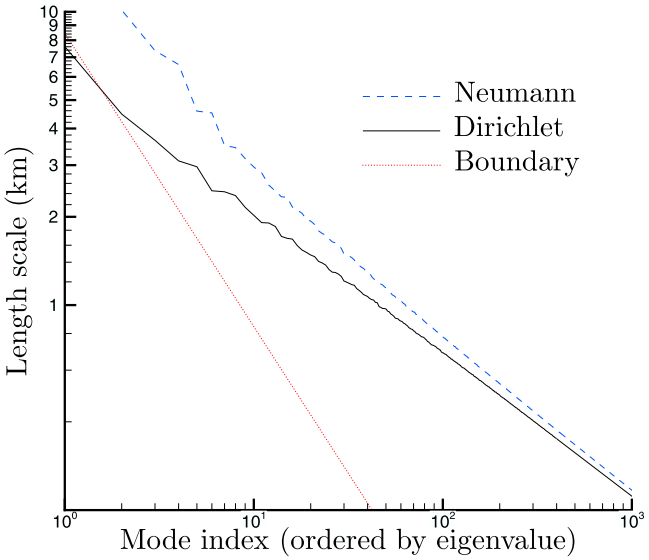

Figure 9. Length scale for the Dirichlet, Neumann, and boundary modes in the Gulf of Eilat using the approximation $L_{\text{avg}}^{\text{rect}}$. By drawing a horizontal line at the desired resolution on this plot, one determines the number of modes needed in each sequence of modes.

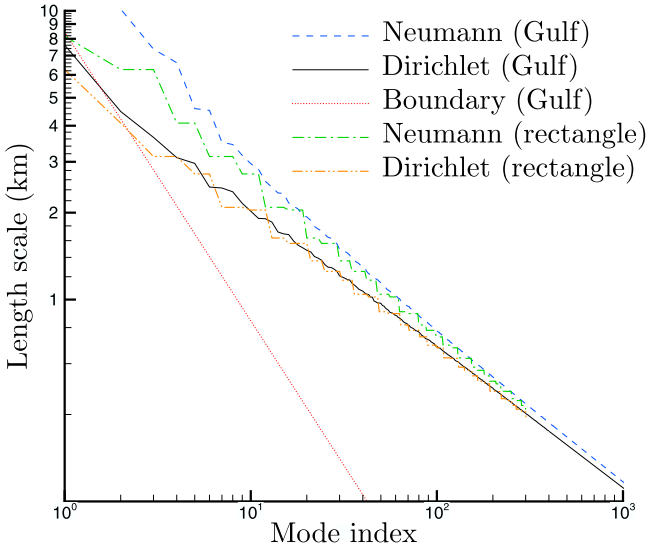

Figure 10. Comparison of the modal length scales for OMA modes in the Gulf of Eilat and the Fourier modes of the rectangle approximating the gulf.

approximated using the closest rectangle. On the basis of the method described in section 4, we have determined that a rectangle of 8.17 km by 6.26 km has the same moment of inertia as the Gulf of Eilat. For the rectangle, one can easily plot the length scale of the Fourier modes as a function of the mode index. Figure 10 compares the length scales for the modes in the gulf and the Fourier modes. Clearly, the length scales of the Fourier modes corroborates our computations in the gulf and can be used as an approximation of the length scale. This conclusion becomes very important when one works with very large sequences of modes. In this case, the eigenvalues of the modes and our length scale approximation may become imprecise when $n \to +\infty$. The behavior of the Fourier modes for the closest rectangle can be used to verify the results or to extrapolate the curves for large n.

[101] Given a set of Dirichlet modes ψ_i ($i = 1 \cdots n_\psi$), a set of Neumann modes ϕ_j ($j = 1 \cdots n_\phi$), and a set of boundary modes ϕ_k^b ($k = 1 \cdots n_b$), the nowcast (i.e., the reconstructed velocity field) is a linear combination of all the modes. The velocity at point $\mathbf{x}$ is given by

$$\mathbf{v}(\mathbf{x}) = \sum_{i=1}^{n_\psi} \alpha_i \nabla \times (\mathbf{k}\,\psi_i(\mathbf{x})) + \sum_{j=1}^{n_\phi} \beta_j \nabla \phi_j(\mathbf{x}) + \sum_{k=1}^{n_b} \gamma_k \nabla \phi_k^b(\mathbf{x}). \tag{8}$$

To perform the nowcast, one needs to determine the coefficients α_i, β_j, and γ_k in such a way that the linear combination best represents the measured radar data. This is typically done by defining a cost function, such as

$$\Phi_{\text{tot}} = \sum_{\nu=1}^{N} \| \mathbf{v}(\mathbf{x}_\nu) - \mathbf{v}_\nu \|^2,$$

where N is the number of total vectors in the radar data, $\mathbf{x}_\nu$ is the position of the ν^{th} measurement and $\mathbf{v}_\nu$ is the ν^{th} total vector. When assimilating radial measurements (as opposed to total vectors), the data set is a sequence of N radial angles θ_ν and the corresponding radial currents v_ν. As depicted by *Kaplan and Lekien* [2007], a cost function for radial data assimilation is given by

$$\Phi_{\text{rad}} = \sum_{\nu=1}^{N} \| \mathbf{1}_{\theta_\nu} \cdot \mathbf{v}(\mathbf{x}_\nu) - v_\nu \|^2,$$

where $\mathbf{1}_{\theta_\nu}$ is the unit vector oriented along the νth radial θ_ν. In both cases the cost function is the difference between the nowcast (reconstructed velocity field which depends on the coefficients α_i, β_j and γ_k) and the observed velocity components. We view this cost as a function of the coefficients α_i, β_j and γ_k and the nowcast is obtained by minimizing the cost function. The corresponding optimal coefficients α_i, β_j and γ_k determine the linear combination of the selected modes that best fit the data [*Lekien et al.*, 2004].

[102] In practice, however, *Kaplan and Lekien* [2007] showed that two critical improvements must be brought to the cost function. First, each term must be weighted inversely proportional to the local measurement density. This modification aims at avoiding the lack of sensitivity of the cost function to regions where data collection is sparse. The second major modification is the introduction of a smoothing term which forces the minimum to correspond to coefficients α_i, β_j and γ_k of reasonable magnitude. Indeed, *Kaplan and Lekien* [2007] showed that without any smoothing term, unphysical large coefficients could correspond to

Table 1. Resolution and Number of Modes Used for Current Reconstruction

Resolution	n_ψ	n_ϕ	n_b	Total Number of Modes (N)
2 km	11	18	5	34
1 km	46	62	9	117
600 m	134	163	14	311
400 m	307	354	22	683

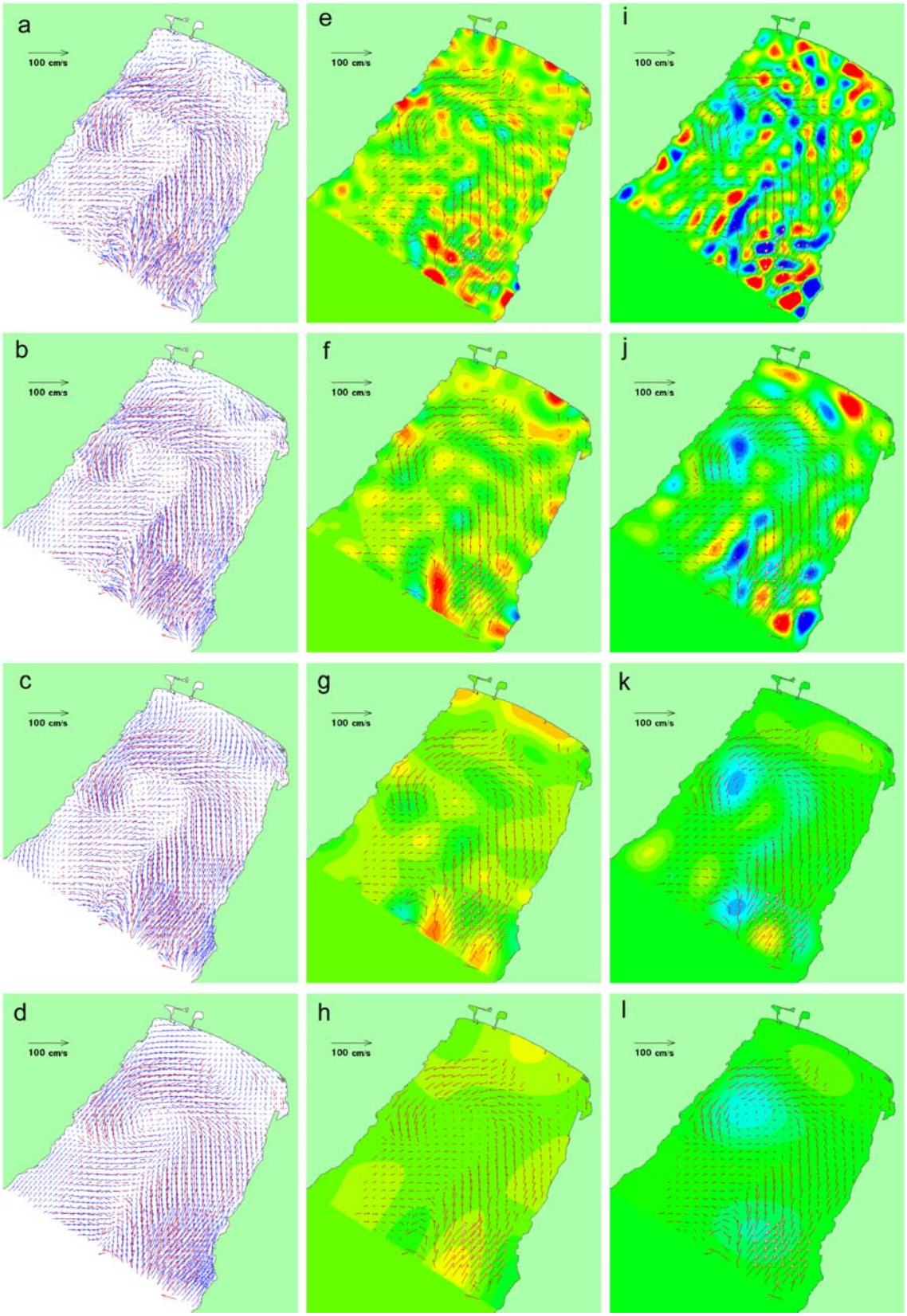

Figure 11. OMA nowcast on 29 November 2005 at 1000 UT based on radial data. (a–d) Recombined total vectors (red) and reconstructed OMA currents (blue). (e–h) Reconstructed divergence. (i–l) Reconstructed vorticity. The nowcast resolution is 400 m (683 modes) in Figures 11a, 11e, and 11i; 600 m (311 modes) in Figures 11b, 11f, and 11j; 1 km (117 modes) in Figures 11c, 11g, and 11k; and 2 km (34 modes) in Figures 11d, 11h, and 11l.

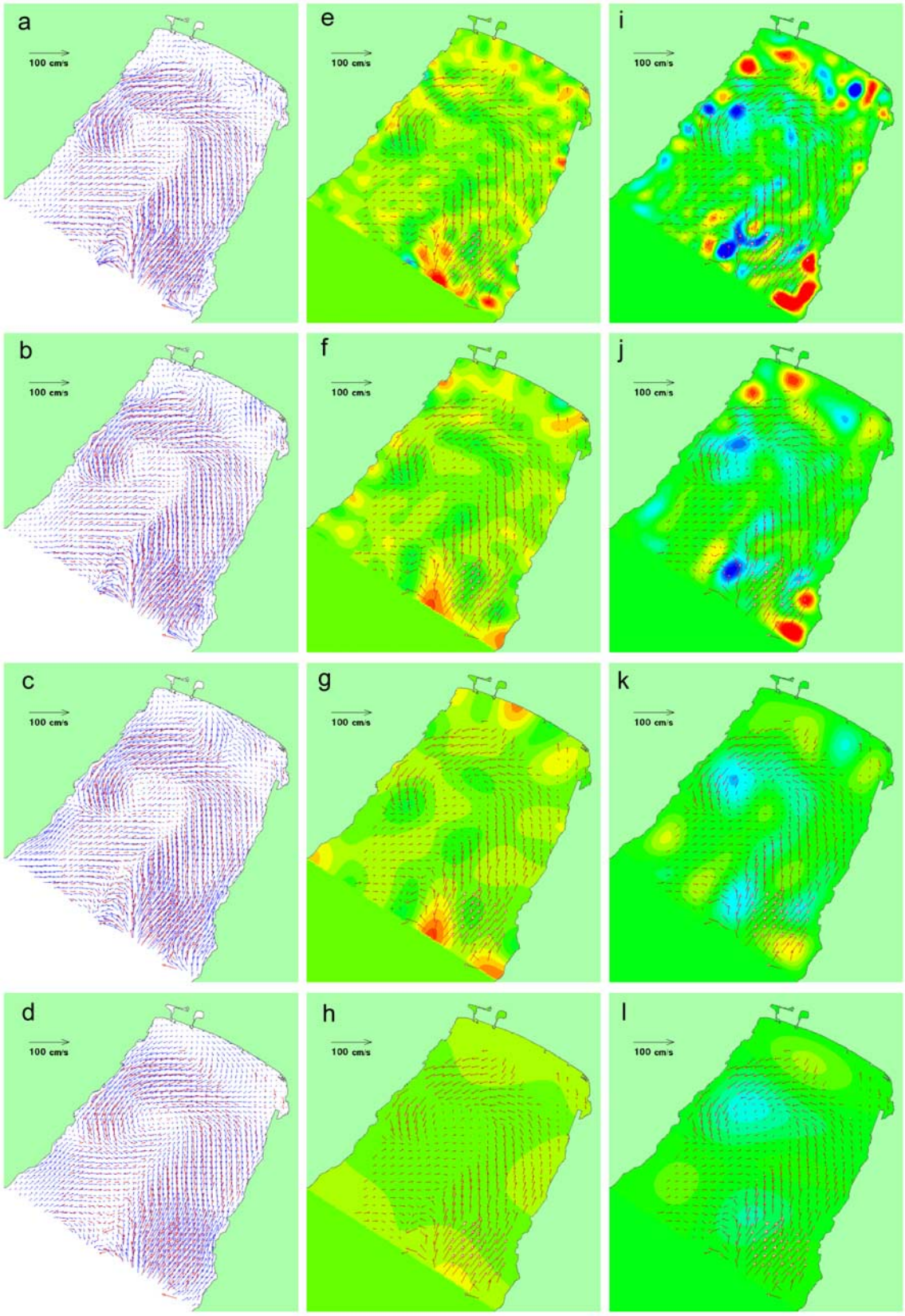

Figure 12. OMA nowcast on 29 November 2005 at 1000 UT based on total data. (a–d) Recombined total vectors (red) and reconstructed OMA currents (blue). (e–h) Reconstructed divergence. (i–l) Reconstructed vorticity. The nowcast resolution is 400 m (683 modes) in Figures 12a, 12e, and 12i; 600 m (311 modes) in Figures 12b, 12f, and 12j; 1 km (117 modes) in Figures 12c, 12g, and 12k; and 2 km (34 modes) in Figures 12d, 12h, and 12l.

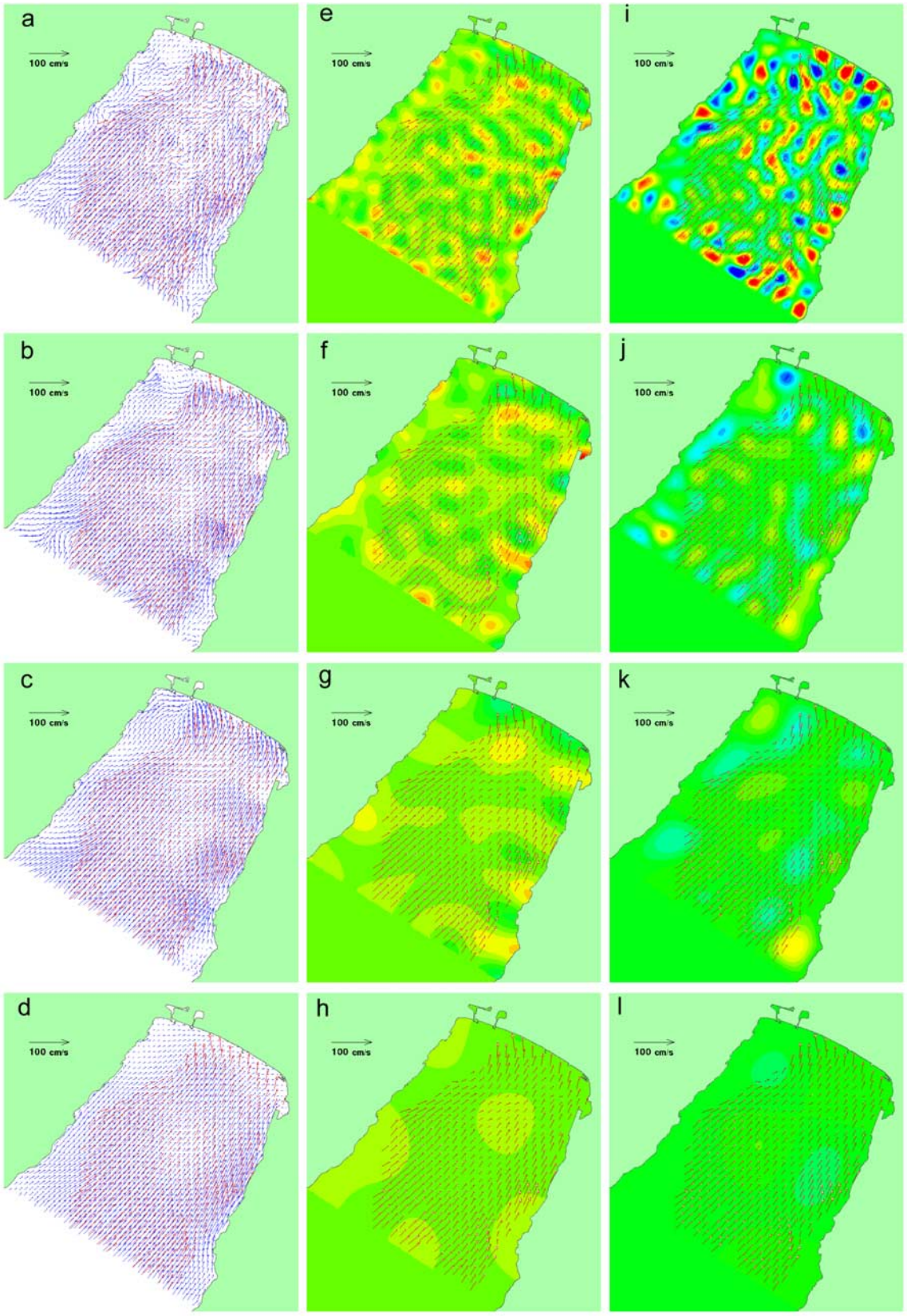

Figure 13. OMA nowcast on 22 June 2006 at 1430 UT based on radial data. (a–d) Recombined total vectors (red) and reconstructed OMA currents (blue). (e–h) Reconstructed divergence. (i–l) Reconstructed vorticity. The nowcast resolution is 400 m (683 modes) in Figures 13a, 13e, and 13i; 600 m (311 modes) in Figures 13b, 13f, and 13j; 1 km (117 modes) in Figures 13c, 13g, and 13k; and 2 km (34 modes) in Figures 13d, 13h, and 13l.

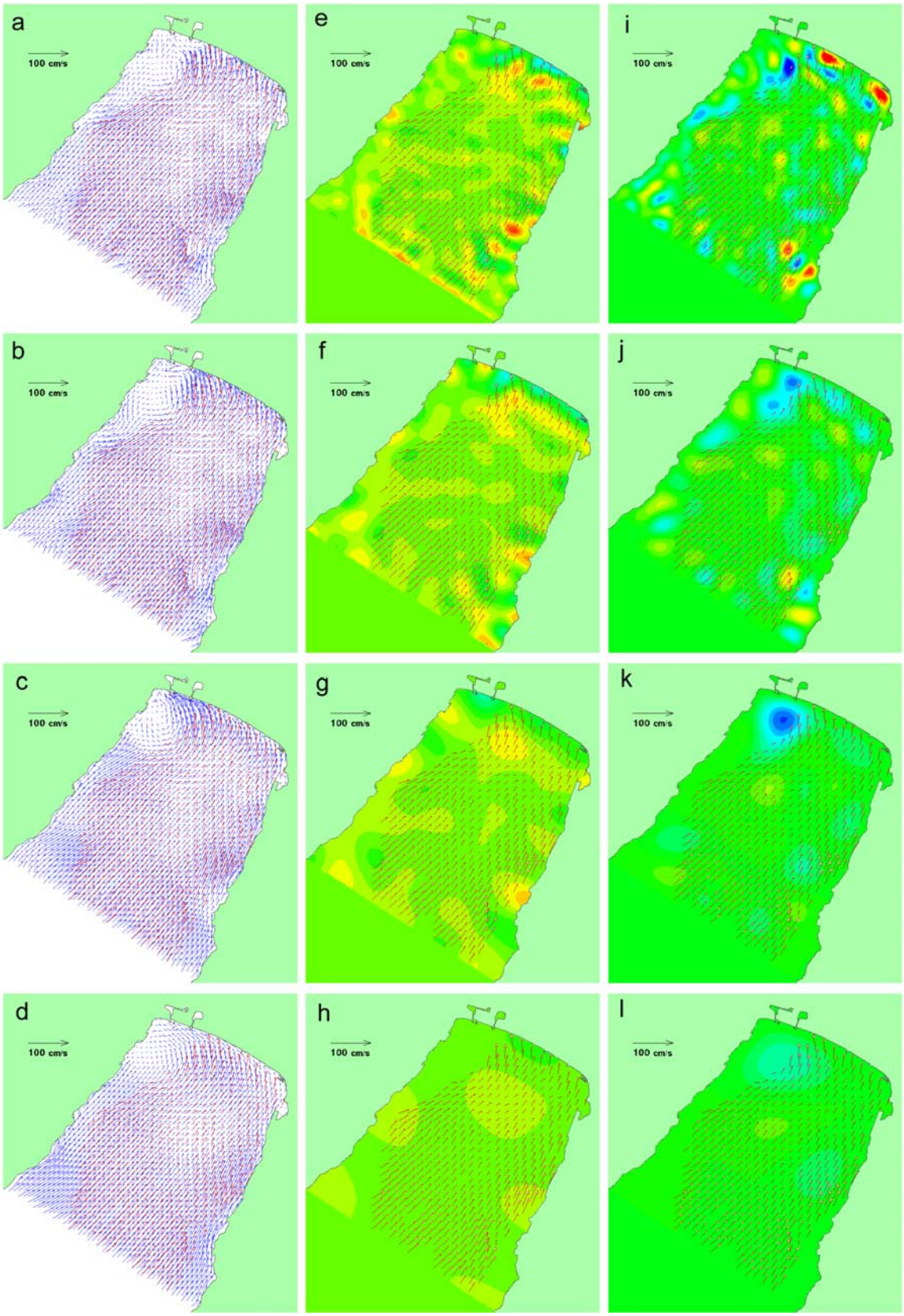

Figure 14. OMA nowcast on 22 June 2006 at 1430 UT based on total data. (a–d) Recombined total vectors (red) and reconstructed OMA currents (blue). (e–h) Reconstructed divergence. (i–l) Reconstructed vorticity. The nowcast resolution is 400 m (683 modes) in Figures 14a, 14e, and 14i; 600 m (311 modes) in Figures 14b, 14f, and 14j; 1 km (117 modes) in Figures 14c, 14g, and 14k; and 2 km (34 modes) in Figures 14d, 14h, and 14l.

the minimum error for a set of radar measurements. These coefficients lead to unphysical large velocity vectors away from the cloud of measurements. The updated cost function for radial measurements is given by

$$\Phi = \sum_{\nu=1}^{N} \underbrace{\frac{1}{A_\nu}}_{\text{weights}} \parallel \mathbf{1}_{\theta_\nu} \cdot \mathbf{v}(\mathbf{x}_\nu) - v_\nu \parallel^2 + \underbrace{K\left(\sum_{i=1}^{n_\psi} \alpha_i^2 + \sum_{j=1}^{n_\phi} \beta_j^2 + \sum_{k=1}^{n_h} \gamma_k^2\right)}_{\text{smoothing}}, \quad (9)$$

where $K = 10^{-9}$ is a smoothing coefficient and A_ν is the inverse of the measurement density at $\mathbf{x}_\nu$ (in this manuscript, the coefficients A_ν are equal to the area of the Voronoi cell of the ν^{th} measurement). Note that other cost functions than the one above can be used. For, example, in the work by *Chu et al.* [2003], the weights are modified to take into account an evaluation of the error at each point. Recently, *Kim et al.* [2008] presented a general optimal interpolation method to compute surface currents from radials, which can be used with either regular grid interpolation or with OMA expansion. When used in conjunction with OMA, the method of *Kim et al.* [2008] provides directly the coefficients α_i, β_j and γ_k and associated errors without the need for using the cost function above. In this manuscript, however, we concentrate on studying the effect of length scales and we derive the OMA coefficients from the quadratic cost function in equation (9), so as to eliminate variations due to other factors.

[103] Given the radar data and a set of modes, we minimize the cost function given in equation (9) to obtain the coefficients α_i, β_j and γ_k. Once the coefficients are computed, the velocity, divergence and vorticity can be computed everywhere using the linear combination in equation (8). Figures 11–14 show the OMA nowcast at the 4 selected resolutions. Figures 11 and 12 are performed for 29 November 2005 at 1000 UT. Figures 13 and 14 analyze the data for 22 June 2006 at 1430 UT.

[104] To study the influence of the input data set, we have performed two OMA nowcast for each date. Figures 11 and 13 assimilate the radial current data. In Figures 12 and 14, we used recombined total vectors as input.

[105] The velocity nowcasts are in good agreement: they are similar whether radial data or total data were used and they are qualitatively similar for all resolutions. It is worth noting that all the nowcasts are compared to the total vectors, hence the nowcast based on radial data may appear less accurate. In fact, OMA nowcasts based on radial data are more accurate: they use more data points and avoid the difficulties and errors due to the process of recombining radial data into total vectors. Detailed analysis of the residual error and more extensive comparisons are given by *Kaplan and Lekien* [2007].

[106] Another important aspect of the nowcasts in Figures 11–14 is our apparent inability to reconstruct divergence and vorticity fields. As we increase the resolution, small features of increasing magnitude keep appearing. In the next section, we compute the energy spectrum and we uncover why, in this case, we can reconstruct the velocity field, but not the divergence and the vorticity field.

8. Energy Spectrum in the Gulf of Eilat

[107] The modal decomposition given in equation (8) is analogous to a Fourier transform. It gives the velocity field as an infinite sum of components, each with a specific length scale. Using the coefficients α_i, β_j, and γ_k, together with the knowledge of the length scale of the corresponding modes, we can then reconstruct the energy spectrum.

[108] In a Fourier transform, each direction has its own wave number (k_x and k_y). One can then either plot a two-dimensional energy spectrum or combine the two directions using the scalar wave number $k = \sqrt{k_x^2 + k_y^2}$. For OMA modes, the anisotropic plot is not currently an option since the modes are not associated with multiple index wave numbers. Each OMA mode accounts for a single wave number $k = \frac{2\pi}{L}$, where L denotes the unique length scale. A disadvantage of using OMA modes to compute energy spectrum is therefore its current inability to identify anisotropic processes (such as alongshore and cross-shelf variations). On the other hand, OMA is a powerful tool for computing isotropic energy spectrum with a single scalar wave number. Indeed, the OMA modes contain features whose length scales are all close to a single reference length scale (see, e.g., Figure 5). In comparison, a Fourier transform does not provide such a length scale segregation. For example, the Fourier mode $\sin(k_x x)\ \sin(k_y y)$ is typically associated with the scalar wave number $k = \sqrt{k_x^2 + k_y^2}$ but when k_x and k_y are much different, this mode spans a large range of length scales.

[109] We define $E(k)\ \mathrm{d}k$ as the quantity of energy contained in modes whose wave numbers are in the interval $[k, k + \mathrm{d}k]$. To illustrate the computation of the spectrum, we consider the month of July 2005. We can compute the average velocity field during month of July by averaging the nowcast coefficients. We then subtract the average of each coefficient to study the fluctuations. The resulting energy spectrum is shown in Figure 15. Linear regression of the data and Scheffé's simultaneous confidence bands [*Seber*, 1977; *Kosorok and Qu*, 1999] reveal $k^{-5/3}$ behavior over the range [400 m, 3 km] that we studied. Such a spectrum is typical for established turbulence but, as far as we know, not for in situ current measurements using HF radar. The evolution of the flow field toward the fully developed turbulence state will be studied in the future.

[110] The energy spectrum $E(k) \sim k^{-5/3}$ decreases with the wave number. Accordingly, the magnitude of the velocity, given by $\sqrt{k\,E(k)} \sim k^{-1/3}$, is therefore also decreasing with k. This explains why the velocity nowcast of the previous section are not sensitive to the number of modes used. Provided that sufficiently many modes are used, the large-scale velocity field is invariant if we add more modes.

[111] On the other hand, the velocity gradient does not decrease with the wave number [*Lekien and Coulliette*, 2007]. Indeed, the magnitude of the derivative of the velocity behaves as $k\sqrt{k\,E(k)} \sim k^{2/3}$. Figure 16 shows the distribution of the velocity gradient across wave numbers and corroborates the fact that the velocity gradient is higher at small scales. This explains why we cannot properly characterize

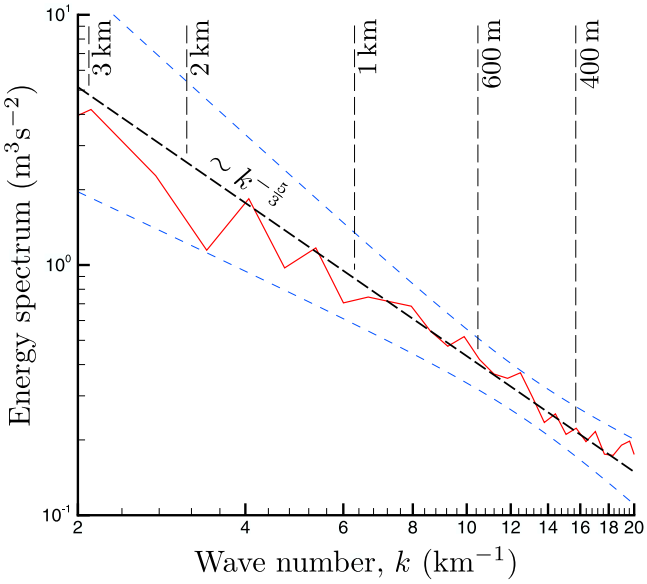

Figure 15. Solid curve indicates energy spectrum for the Gulf of Eilat based on OMA nowcasts (July 2005). Dashed line indicates least square linear regression which gives the slope $-1.53\ldots \approx -\frac{5}{3}$. Light dashed curves indicate 90% confidence bands for the linear regression [*Seber*, 1977].

vorticity and divergence in the nowcast of the previous section. As we increase the resolution of the OMA nowcast, the minimum length scale decreases and we find smaller-scale features in the vorticity and in the divergence, with magnitudes higher than that of the large scale. As a result, the estimates of the vorticity and divergence should be viewed with caution as it varies with the selected nowcast resolution [*Ramp et al.*, 2008].

[112] This result is also critical for Lagrangian studies. Whether one studies a drifting body or the evolution of a tracer, the velocity gradient creates significant stretching and induces particle separation [*Lekien and Haller*, 2008]. We cannot ignore small-scale features in the velocity gradient if its magnitude does not decrease with k. When studying advection and Lagrangian properties, velocity fields must be reconstructed with a large number of OMA modes. Using only few modes may lead to an acceptable qualitative velocity field, but a long sequence of modes is needed to capture the significant amount of velocity gradient at the small scales.

9. Conclusion

[113] In this paper, we analyzed the modes used in the open-boundary modal analysis (OMA) method and determined synoptic length scales for each mode. The length scale of an OMA mode depends on the features of the mode (width of the eddies, position of the saddle points, ...) and is difficult to compute, in particular for large mode indexes. For this reason, we have also derived approximated formula that give the mode length scale as a function of quantities that are more readily available (such as the number of eddies or the number of saddle points for the most accurate formula, or only the mode index and the mode eigenvalue for the most convenient formula).

[114] We have tested the approximated length scale formula on rectangular domains of various aspect ratio. In addition, the quantities are also compared for the Gulf of Eilat, a nearly rectangular domain, where we find excellent agreement.

[115] The new approximated length scales gave us the ability to improve the performances of OMA techniques for two specific applications. First, we are better equipped to select appropriate modes that correspond to all the length scales below a certain threshold. As a result, the OMA nowcasts that result from the projection of the HF radar data on the selected OMA modes are more accurate and filtered with a precise scale. Second, we are now able to compute very accurate energy spectra for coastal regions using OMA modes. Whether the flow is laminar, quasi-turbulent, or turbulent, we can reconstruct the energy density as a function of the length scale for any length scale where there is a sufficiently strong HF radar signal. Using the approximated formula is particularly efficient when studying the asymptotic behavior of the energy spectrum. Indeed, all the approximated length scale formula presented in this paper are asymptotically approaching the synoptic length scale. For small length scales (that is, for large wave numbers), behavior with respect to an approximated wave number is therefore identical to the behavior with respect to the synoptic wave number.

[116] It is also worth noting that the new developments in this manuscript did not provide much improvement in reconstructing the divergence and vorticity fields in the quasi-turbulent Gulf of Eilat. While the nowcast of the surface currents improved, the vorticity and divergence fields remain strongly influenced by the selected scale threshold. This is a fundamental issue due to the fact that

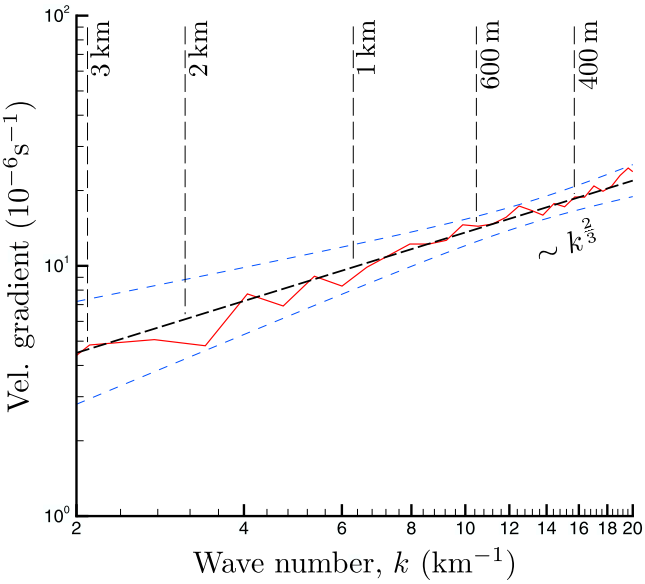

Figure 16. Solid curve indicates magnitude of the velocity gradient in the Gulf of Eilat based on the OMA nowcast (July 2005). Dashed line indicates least square linear regression which gives a slope $0.688\ldots \approx \frac{2}{3}$. Light dashed curves indicate 90% confidence bands for the linear regression [*Seber*, 1977].

the energy does not decrease fast enough in quasi-turbulent flows. As shown by *Lekien and Coulliette* [2007], quantities based on derivatives of the velocity (such as velocity gradient, divergence and vorticity) are often distributed over a wide range of length scales and can hardly be reconstructed by a set of modes filtering high wave numbers. This phenomena is critical in understanding transport and mixing in quasi-turbulent flows [see, e.g., *Mathur et al.*, 2007] and further research is planned to understand and overcome this phenomena.

[117] The aim of this manuscript is to associate a length scale with each mode. Given a prescribed cutoff length scale, our formulas can determine efficiently and accurately which modes must be included in the nowcast. We did not, however, address the question of how to select the cutoff. Indeed, in addition to geometric considerations, the choice depends on external factors such as native resolution and noise levels in the HF radar data.

Notation

Domain and geometries

- $\Omega \subset \mathbb{R}^2$ Domain of interest.
- $\mathrm{Area}(\Omega)$ Area of the domain Ω.
- $\partial\Omega$ Boundary of the domain.
- $\partial\Omega_0$ Portion of boundary made of "solid coastline." $\mathbf{n} \cdot \mathbf{v} = 0$ on $\partial\Omega_0$.
- $\partial\Omega_1$ Open boundary where in/outflow is allowed. $\partial\Omega_1 = \partial\Omega \backslash \partial\Omega_0$.
- $\mathbf{n}$ Unit vector normal to the boundary $\partial\Omega$ and pointing outward.
- L Length (largest side) of the domain. If the domain Ω is not a rectangle, L is the length of the rectangle that has the same area and the same moment of inertia tensor as Ω.
- W Width (shortest side) of the domain. If the domain Ω is not a rectangle, W is the width of the rectangle that has the same area and the same moment of inertia tensor as Ω.
- $r = \frac{L}{W}$ Aspect ratio of the domain. Without loss of generality, $r \geq 1$.

Modes and eigenvalues

- ψ_{ij} Dirichlet Fourier mode: $\psi_{ij} = \sin(i\pi\frac{x}{L}) \sin(j\pi\frac{y}{W})$.
- ϕ_{ij} Neumann Fourier mode: $\phi_{ij} = \cos(i\pi\frac{x}{L}) \cos(j\pi\frac{y}{W})$.
- $-\lambda_{ij}^2$ Eigenvalue of a Fourier mode: $-\lambda_{ij}^2 = -\pi^2 (\frac{i^2}{L^2} + \frac{j^2}{W^2})$.
- ψ_n nth Dirichlet mode on a domain Ω: $\Delta\psi_n = -\lambda_n^2 \psi_n$ in Ω. $\psi_n = 0$ on $\partial\Omega$.
- ϕ_n nth Neumann mode on a domain Ω: $\Delta\phi_n = -\lambda_n^2\phi_n$ in Ω. $\mathbf{n} \cdot \nabla\phi_n = 0$ on $\partial\Omega$.
- $-\lambda_n^2$ Eigenvalue of the nth Dirichlet or Neumann mode. The eigenvalues are referred to as "$-\lambda_n^2$" since, for both problems, they are real and negative.
- ϕ_n^b nth open-boundary mode on a domain Ω. $\Delta\phi_n^b = \frac{\oint_{\partial\Omega} g_n(s)\, \mathrm{d}s}{\mathrm{Area}(\Omega)}$ in Ω. $\mathbf{n} \cdot \nabla\phi_n^b = g_n(s)$ on $\partial\Omega$.

Eddy length scales

- $l_{\min}$ Width (smallest dimension) of the eddy.
- l_h Length (largest dimension) of the eddy.
- $l_{\max}$ Diameter of the eddy.
- $\bar{l}$ Square root of the area of the eddy.

Modal length scales

- N_c Number of eddies in a mode.
- μ_k Length scale of the kth eddy.
- $L_{\min}$ Minimum eddy length scale. $L_{\min} = \min_k\{\mu_k\}$.
- $L_{\max}$ Maximum eddy length scale. $L_{\max} = \max_k\{\mu_k\}$.
- L_{avg} Average eddy length scale. $L_{\mathrm{avg}} = \frac{1}{N_c}\sum_{k=1}^{N_c} \mu_k$.
- L_{rms} RMS eddy length scale. $L_{\mathrm{rms}} = \sqrt{\frac{1}{N_c}\sum_{k=1}^{N_c} \mu_k^2}$

Approximated length scales

- L^{LKG00} Lower bound [from *Lipphardt et al.*, 2000]. $L^{\mathrm{LKG00}} = \frac{\pi}{\lambda}$.
- L^{up} Upper bound. $L^{\mathrm{up}} = \sqrt{2}\,\frac{\pi}{\lambda}$.
- L^{LCBM04} Dimensional approximation [from *Lekien et al.*, 2004]. $L^{\mathrm{LCBM04}} = \nu\, W \frac{\lambda_1}{\lambda}$. $\nu = 1$ (Dirichlet) or $\nu = \sqrt{1 + r^2}$ (Neumann).
- L^{rect} Exact length scale for the closest rectangle. $L^{\mathrm{rect}} = \sqrt{2}\,\frac{\pi}{\lambda}\left(1 + \sqrt{1 - \frac{4\,\pi^4\,N_c^2}{\lambda^4\,\mathrm{Area}^2(\Omega)}}\right)^{-\frac{1}{2}}$. N_c = number of eddies (Dirichlet) or saddles (Neumann). This formula gives the exact length scale for Fourier modes but requires the difficult computation of N_c.
- $L_{\max}^{\mathrm{rect}}$ Same as L^{rect} but N_c is replaced by its upper bound. $L_{\max}^{\mathrm{rect}} = \sqrt{2}\,\frac{\pi}{\lambda} = L^{\mathrm{up}}$.
- $L_{\min}^{\mathrm{rect}}$ Same as L^{rect} but N_c is replaced by its lower bound. $L_{\min}^{\mathrm{rect}} = \sqrt{2}\,\frac{\pi}{\lambda}\left(1 + \sqrt{1 - \frac{4\pi^2}{\lambda^2\, r\,\mathrm{Area}^2(\Omega)}}\right)^{-\frac{1}{2}}$.
- $L_{\mathrm{avg}}^{\mathrm{rect}}$ Same as L^{rect} but N_c is replaced by its average value. $L_{\mathrm{avg}}^{\mathrm{rect}} = \frac{\pi}{\lambda}\frac{2}{\sqrt{2 + \sqrt{3 - \frac{4\pi^2}{\lambda^2\, r\,\mathrm{Area}(\Omega)} - \frac{4\pi}{\lambda\sqrt{r\,\mathrm{Area}(\Omega)}}}}}$.
- $L_{\gamma}^{\mathrm{rect}}$ Same as L^{rect} but N_c is replaced by the γ estimate (see first two equations in paragraph 86). $L_{\gamma}^{\mathrm{rect}} = \sqrt{2}\,\frac{\pi}{\lambda}\left(1 + \sqrt{1 - \frac{4\,\pi^4\,\gamma^2(n)}{\lambda^4\,\mathrm{Area}^2(\Omega)}}\right)^{-\frac{1}{2}}$ where n is the mode index.

[118] **Acknowledgments.** We are grateful to David M. Kaplan (UCSC) and Donald E. Barrick (CODAR Ocean Sensors Ltd.) for enlightening discussions. The OMA modes used and shown in this manuscript were computed using the software package OMA (http://www.lekien.com/~francois/software/oma). Linear eigenvalue problems and linear equations are solved using ARPACK, LAPACK, and UMFPACK. H.G. is the incumbent of the Rowland and Sylvia Schaefer Career Development Chair and is supported by a research grant from the Estate of Sanford Kaplan. This research was partially supported by the Israel Science Foundation (grant 781/04) and by NATO (project SfP982220).

References

Arnoldi, W. E. (1951), The principle of minimised iteration in the solution of the matrix eigenvalue problem, *Q. Appl. Math.*, *9*, 17–29.

Aubin, J.-P. (2000), *Applied Functional Analysis*, 2nd ed., John Wiley, New York.

Barrick, D. E. (2002), Geometrical dilution of statistical accuracy (GDOSA) in multi-static HF radar networks, CODAR Ocean Sensors, Mountain View, Calif. (Available at http://www.codaros.com/Manuals/SeaSonde/Docs/Informative/GDOSA_Definition.pdf)

Barrick, D. E., M. W. Evans, and B. L. Webber (1977), Ocean surface currents mapped by radar, *Science*, *198*, 138–144, doi:10.1126/science.198.4313.138.

Barrick, D. E., B. J. Lipa, and R. D. Crissman (1985), Mapping surface currents with CODAR, *Sea Technol.*, *26*(10), 43–48.

Buckingham, E. (1914), On physically similar systems: Illustrations of the use of dimensional equations, *Phys. Rev.*, *4*, 345–376.

Chu, P. C., L. M. Ivanov, T. P. Korzhova, T. M. Margolina, and V. M. Melnichenko (2003), Analysis of sparse and noisy ocean current data using flow decomposition, *J. Atmos. Oceanic Technol.*, *20*, 478–491.

Coulliette, C., F. Lekien, J. D. Paduan, G. Haller, and J. E. Marsden (2007), Optimal pollution mitigation in Monterey Bay based on coastal radar data and nonlinear dynamics, *Environ. Sci. Technol.*, *41*(18), 6562–6572, doi:10.1021/es0630691.

Courant, R., and D. Hilbert (1953), *Methods of Mathematical Physics*, vol. I, Interscience, New York.

Curtis, W. D., J. D. Logan, and W. Parker (1982), Dimensional analysis and the Π theorem, *Linear Algebra Appl.*, *47*, 117–126.

Dieci, L., and T. Eirola (1999), On smooth decompositions of matrices, *SIAM J. Matrix Anal. Appl.*, *20*(3), 800–819.

Eremeev, V. N., L. M. Ivanov, A. D. Kirwan, and T. M. Margolina (1992a), Reconstruction of oceanic flow characteristics from quasi-Lagrangian data: 1. Approach and mathematical methods, *J. Geophys Res.*, *97*(C6), 9733–9742.

Eremeev, V. N., L. M. Ivanov, A. D. Kirwan, T. M. Margolina, O. V. Melnichenko, S. V. Kochergin, and R. R. Stanichnaya (1992b), Reconstruction of oceanic flow characteristics from quasi-Lagrangian data: 2. Characteristics of the large-scale circulation in the Black Sea, *J. Geophys Res.*, *97*(C6), 9743–9753.

Gildor, H., E. Fredj, J. Steinbuck, and S. Monismith (2009), Evidence for submesoscale barriers to horizontal mixing in the ocean from current measurements and aerial-photographs, *J. Phys. Oceanogr.*, doi:10.1175/2009JPO4116.1, in press.

Golub, G. H., and C. F. Van Loan (1996), *Matrix Computations*, 3rd ed., Johns Hopkins Univ. Press, Baltimore, Md.

Guckenheimer, J., and P. J. Holmes (1983), *Nonlinear Oscillations, Dynamical Systems, and Bifurcations of Vector Fields*, Springer, New York.

Gurgel, K. W., G. Antonischki, H. H. Essen, and T. Schlick (1999a), Wellen Radar (WERA): A new ground-wave HF radar for ocean remote sensing, *Coastal Eng.*, *37*(3–4), 219–234.

Gurgel, K. W., H. H. Essen, and S. P. Kingsley (1999b), High-frequency radars: Physical limitations and recent developments, *Coastal Eng.*, *37*(3–4), 201–218.

Hodgins, D. O. (1994), Remote-sensing of ocean surface currents with the SeaSonde HF radar, *Spill Sci. Technol. Bull.*, *1*, 109–129.

Kaplan, D. M., and F. Lekien (2007), Spatial interpolation and filtering of surface current data based on open-boundary modal analysis, *J. Geophys. Res.*, *112*, C12007, doi:10.1029/2006JC003984.

Kim, S., E. Terrill, and B. Cornuelle (2007), Objectively mapping HF radar-derived surface current data using measured and idealized data covariance matrices, *J. Geophys. Res.*, *112*, C06021, doi:10.1029/2006JC003756.

Kim, S., E. J. Terrill, and B. D. Cornuelle (2008), Mapping surface currents from HF radar radial velocity measurements using optimal interpolation, *J. Geophys. Res.*, *113*, C10023, doi:10.1029/2007JC004244.

Kosorok, M. R., and R. Qu (1999), Exact simultaneous confidence bands for a collection of univariate polynomials in regression analysis, *Stat. Med.*, *18*, 63–620, doi:10.1029/2007JC004244.

Lehoucq, R. B., D. C. Sorensen, and C. Yang (1998), *ARPACK Users' Guide: Solution of Large-Scale Eigenvalue Problems with Implicitly Restarted Arnoldi Methods*, Soc. for Indust. and Appl. Math., Philadelphia. Pa.

Lekien, F., and C. Coulliette (2007), Chaotic stirring in quasi-turbulent flows, *Philos. Trans. R. Soc. A*, *365*, 3061–3084.

Lekien, F., and G. Haller (2008), Unsteady flow separation on slip boundaries, *Phys. Fluids*, *20*, 097101.

Lekien, F., C. Coulliette, R. Bank, and J. E. Marsden (2004), Open-boundary modal analysis: Interpolation, extrapolation, and filtering, *J. Geophys. Res.*, *109*, C12004, doi:10.1029/2004JC002323.

Lekien, F., C. Coulliette, A. J. Mariano, E. H. Ryan, G. Haller, and J. Marsden (2005), Pollution release tied to invariant manifolds: A case study for the coast of Florida, *Physica D*, *210*(1–2), 1–20, doi:10.1016/j.physd.2005.06.023.

Lipphardt, B. L., Jr., A. D. Kirwan Jr., C. E. Grosch, J. K. Lewis, and J. D. Paduan (2000), Blending HF radar and model velocities in Monterey Bay through normal mode analysis, *J. Geophys. Res.*, *105*(C2), 3425–3450.

Lipphardt, B. L., Jr., D. Small, A. D. Kirwan Jr., S. Wiggins, K. Ide, C. E. Grosch, and J. D. Paduan (2006), Synoptic Lagrangian maps: Application to surface transport in Monterey Bay, *J. Mar. Res.*, *64*(2), 221–247.

Lynch, P. (1989), Partitioning the wind in a limited domain, *Mon. Weather Rev.*, *117*, 1492–1500.

Mathur, M., G. Haller, T. Peacock, J. E. Ruppert-Felsot, and H. L. Swinney (2007), Uncovering the Lagrangian skeleton of turbulence, *Phys. Rev. Lett.*, *98*(14), 144502.

Olascoaga, M. J., I. I. Rypina, M. G. Brown, F. J. Beron-Vera, H. Koak, L. E. Brand, G. R. Halliwell, and L. K. Shay (2006), Persistent transport barrier on the West Florida Shelf, *Geophys. Res. Lett.*, *33*, L22603, doi:10.1029/2006GL027800.

Paduan, J. D., and L. K. Rosenfeld (1996), Remotely sensed surface currents in Monterey Bay from shore-based HF radar (coastal ocean dynamics application radar), *J. Geophys. Res.*, *101*(C9), 20,669–20,686.

Ramp, S. R., D. E. Barrick, T. Ito, and M. S. Cook (2008), Variability of the Kuroshio Current south of Sagami Bay as observed using long-range coastal HF radars, *J. Geophys. Res.*, *113*, C06024, doi:10.1029/2007JC004132.

Seber, G. A. (1977), *Linear Regression Analysis*, John Wiley, New York.

Shnirelman, A. I. (1974), Ergodic properties of eigenfunctions, *Usp. Mat. Nauk.*, *29*, 181–182.

Trefethen, L. N., and T. Betcke (2006), Computed eigenmodes of planar regions, in *Recent Advances in Differential Equations and Mathematical Physics*, *Contemporary Math. Ser.*, vol. 412, pp. 297–314, Am. Math. Soc., Providence, R. I.

Tricoche, X., G. Scheuermann, and H. Hagen (2000), Higher order singularities in piecewise linear vector fields, in *The Mathematics of Surfaces IX*, pp. 99–113, Springer, London.

Tricoche, X., G. Scheuermann, and H. Hagen (2001), Continuous topology simplification of planar vector fields, in *Proceedings of the Conference on Visualization '01*, pp. 159–166, Inst. for Electr. and Electron. Eng., Piscataway, N. J.

Weyl, H. (1950), Ramifications of the eigenvalue problem, *Bull. Am. Math. Soc.*, *56*, 115–139.

H. Gildor, Department of Environmental Sciences and Energy Research, Weizmann Institute of Science, Rehovot 76100, Israel. (hezi.gildor@weizmann.ac.il)

F. Lekien, École Polytechnique, Université Libre de Bruxelles, CP 165/11, B-1050 Brussels, Belgium. (lekien@ulb.ac.be)